NMR multiple echoes observed in solid ^{3}He

G. Deville, M. Bernier, and J. M. Delrieux

(Received 4 January 1979; revised manuscript received 18 April 1979)

A large number of echoes—called multiple echoes—following two isolated NMR radio-frequency pulses separated by a time τ, have been observed in bcc ^{3}He. A quantitative theory of this phenomenon is given, taking into account the nonlinear effect of the nuclear demagnetizing field in the equation of motion of the magnetization. In a magnetic-field gradient G, just before the second pulse at time τ, the nuclear-spin transverse magnetization has a helical configuration of pitch $\gamma G\tau = k_0$, which is converted by the second radio-frequency pulse into a sinusoidal modulation of the magnetization along the magnetic field gradient. The corresponding sinusoidal demagnetizing field modulates spatially the NMR resonance frequency so that the transverse magnetization is a superposition of helical configurations with pitch pk_0 (multiple of k_0), yielding multiple echoes at times $p\tau$. A detailed comparison with the experimental results obtained at high temperatures (300 mK $< T <$ 1 K) and low temperatures (1 $< T <$ 20 mK), leads to a satisfactory agreement with the experiments. The main practical application of the multiple-echo study is to provide a method of measurement of the absolute value of the nuclear-spin susceptibility without knowing the shape or the number of spins of the sample. The transverse relaxation time T_2 and the diffusion coefficient D are also obtained with this analysis. When applied to the low-temperature measurements, the multiple-echo analysis has pointed out, for the first time, the increase of the magnetic susceptibility of solid ^{3}He in the paramagnetic phase near the ordering temperature T_c, while in contrast the relaxation times T_1 and T_2 and the diffusion coefficient D do not change appreciably, even just above T_c.

I. INTRODUCTION

In usual NMR pulse experiments, a sequence of two radio-frequency (rf) pulses at times 0 and τ gives a single echo at time 2τ.[1] In recent pulsed NMR experiments in solid ^{3}He, an unusual phenomenon was observed[2–4]: the same two-pulse sequence was followed by a large number of echoes at times $2\tau, 3\tau, 4\tau, \ldots, n\tau, \ldots$. These experiments were first performed at low frequency ($f \simeq 125$ kHz) and low temperature ($T = 1$ to 20 mK). The solid sample, prepared by adiabatic compression (Pomeranchuk cooling) was in equilibrium with the liquid along the melting curve; in these conditions we observed a transition in the solid at $T_c = 1.07$ mK but there were many converging indications that the multiple echoes were not related to this transition: they appeared far from T_c, at temperatures as high as 20 mK; moreover, the same echo pattern was obtained when varying both the magnetic field H_0 and the temperature T such that the ratio H_0/T remained the same. This feature has been corroborated by a new set of experiments performed in solid ^{3}He at higher temperatures ($T \simeq 0.5$ K) and higher fields ($H_0 \simeq 1$ T). In these conditions, solid ^{3}He was in the well-known paramagnetic phase, the low-temperature effects were absent ($T \gg T_c$), and the ratio H_0/T was roughly the same as in the experiments considered above. Large multiple echoes very similar to the low-temperature ones were actually observed in the 1-K range, showing without any doubt that the multiple echoes must be explained within the framework of the paramagnetic phase.

The aim of this paper is to show that multiple echoes are explained quantitatively by the effect of the demagnetizing field $H_d \sim 4\pi M_0$ created by the nuclear-spin magnetization M_0. In conventional NMR this field, being small, has usually a negligible effect compared to that of the external applied field. In solid ^{3}He this is not always true: the large nuclear-spin exchange frequency due to the large zero-point motion of the ^{3}He atoms leads to a motional narrowing of the NMR line and thus to a long transverse relaxation time T_2 ($T_2 \simeq 250$ msec at molar volume $V_m = 24.25$ cm^3). The demagnetizing field H_d acting on the transverse magnetization during a time of the order of T_2, has a significant effect when $\gamma H_d T_2 \gtrsim 1$. This condition is fulfilled in bcc ^{3}He when H_d is of the order of a few tenths of a milligauss. In our low-field experiments ($H_0 = 38.6$ G), this condition is satisfied for temperatures lower than 40 mK. The demagnetizing field is a nonlocal function of the magnetization at each point and introduces complex nonlinear terms in the equation describing the evolution of the sample magnetization.

When applying rf pulses, we change the orientation

of the magnetization with respect to the external field; if the spin system has been prepared in such a way that the initial magnetization is not homogeneous over the sample, an rf pulse produces nonuniform NMR frequency displacements which yield low-frequency beats in the observed magnetization. The effect of the nonlinear terms due to the demagnetizing field can be seen as a mixing of the spatial Fourier components of the magnetization which then do not evolve independently of one another.

The effect of the demagnetizing field on spin systems is actually related to the more general problem of the evolution of nonlinear systems, regardless of the origin of the nonlinear terms. Various kinds of multiple echoes should appear whenever the resonance frequency of a system is a function of the excitation level and thus they could be observed in many physical systems exhibiting echo phenomena, e.g., piezoelectric crystals,[5] type-II superconductors,[6] plasmas,[7] and solids in which the "boson echoes" phenomena[8] can be achieved. In spin systems the same kind of equations for the spin precession as those in solid ^{3}He appears also in uniaxial antiferromagnets.[9] In ferrimagnetic materials[10] a series of multiple echoes is also expected to follow a two-pulse sequence. Let us mention the distinction between two kinds of nonlinearity:

(i) The strong nonlinearity which is active during the pulse and whose effect depends strongly on the strength of the pulse. This is the case in the uniaxial antiferromagnet considered in Ref. 9.

(ii) The weak nonlinearity which acts over the long time between the pulses as is the case in solid ^{3}He. However, in most of these systems strong physical simplifications are necessary to carry out the calculation in detail, whereas for solid ^{3}He the expression for the nonlinear terms is well established. Thus, for solid ^{3}He detailed and exact calculations can be made for certain easily fulfilled experimental conditions, from which we can deduce microscopic parameters like T_2, the spin-diffusion coefficient D, and the absolute value of the magnetic susceptibility χ.

This paper is organized as follows: In Sec. II, we give the physical ideas governing the creation of multiple echoes in pulse experiments and we show that the relation between the magnetization and the demagnetizing field, which is in general nonlocal, becomes a simple local relation in our experimental conditions. We then give an exact solution of the problem in the case where the spin diffusion is negligible, leading to an analytic expression for the amplitude of all the echoes following a two-pulse sequence. Taking into account the diffusion, we then show that the problem can only be solved completely by calculating the evolution of the spatial Fourier components of the magnetization with a computer, the precision obtained for the echo amplitudes being limited only by the computing time.

In Sec. III, we test the validity of the theory by comparison with our experimental results and in particular we show how the parameters χ, T_2, and D are obtained from fitting the experimental curves to the theoretical predictions. Let us mention that the agreement between theory and experiments at low temperature, which was already quite satisfactory neglecting the diffusion effects, as reported in Ref. 2, is significantly improved when these effects are included.[11] In conclusion, we claim that the study of multiple echoes, in solid ^{3}He in particular, but also in other systems, provides a new method for the measurement of the diffusion coefficient, the transverse relaxation time, and especially the absolute value of the nuclear magnetization without knowing the total number of spins in the sample; to our knowledge, this last determination cannot be achieved with any other method.

II. GENERAL THEORY

A. Physical hypothesis of the model

We study the response of solid ^{3}He after two radio-frequency pulses of angles α_1 and α_2 occurring at times 0 and τ. The volution of the magnetization is governed by the nuclear-spin Hamiltonian

$$\mathcal{H} = \mathcal{H}_Z + \mathcal{H}_{ex} + \mathcal{H}_D$$

where $\mathcal{H}_Z = \gamma \hbar H S_z$ is the Zeeman Hamiltonian, $\mathcal{H}_{ex}$ is the exchange Hamiltonian, and

$$\mathcal{H}_D = \sum_{i<j} \frac{\hbar^2\gamma^2}{|\vec{r}_i - \vec{r}_j|^3} \times \left(\vec{S}_i \cdot \vec{S}_j - \frac{3[\vec{S}_i \cdot (\vec{r}_i - \vec{r}_j)][\vec{S}_j \cdot (\vec{r}_i - \vec{r}_j)]}{|\vec{r}_i - \vec{r}_j|^2} \right) \tag{1}$$

is the dipole-dipole Hamiltonian.

The $\mathcal{H}_{ex}$ Hamiltonian has been taken for a long time as an Heisenberg Hamiltonian with a two spin interaction. The experimental behavior of solid ^{3}He at temperatures below 5 mK shows that a more complex Hamiltonian must be considered.[12] Different models have been proposed: four-spin interaction,[13–15] zero-point vacancies,[16] or large spin-phonon coupling.[12,17] Nevertheless, the exact nature of $\mathcal{H}_{ex}$ is not of great importance for the present problem and could even be that of a classical liquid. The unique property used is the motional narrowing of the NMR

line ($\mathcal{H}_{ex} >> \mathcal{H}_D$) so that the transverse relaxation time T_2 is much larger than that observed in the absence of any motion.[18] This property can be expressed by $T_2 \langle \mathcal{H}_D'^2 \rangle^{1/2} >> 1$ if we note by $\langle \mathcal{H}_D'^2 \rangle$ the second moment of the NMR line where $\mathcal{H}_D'$ stands for the secular part of $\mathcal{H}_D$.

This motional narrowing comes from the fact that the motion of the spin on an atomic scale, due to the exchange interaction[19] is about 10^3 times larger than the dipolar interaction on the same atomic scale. Nevertheless, because $\mathcal{H}_D$ is a long-range interaction and $\mathcal{H}_{ex}$ a short-range one, the fluctuations of the relative orientations of two spins due to $\mathcal{H}_{ex}$ become slower and slower as the distance r between these two spins increases, so that, for r larger than a critical value r_c the fluctuations due to $\mathcal{H}_{ex}$ become smaller than that due to the dipolar energy $\mathcal{H}_D$. Thus the long-range effect of the dipolar interaction is not changed by the exchange motional narrowing and consequently this long-range part of $\mathcal{H}_D$ is described by the macroscopic model of a local demagnetizing field

$$\vec{H}_d(\vec{r}) = \int d^3r' \frac{1}{|\vec{r}-\vec{r}'|^3} \times \left[\vec{M}(\vec{r}') - \frac{3[\vec{M}(\vec{r}')\cdot(\vec{r}-\vec{r}')](\vec{r}-\vec{r}')}{|\vec{r}-\vec{r}'|^2} \right], \tag{2}$$

where $\vec{M}(\vec{r})$ is the local magnetization at $\vec{r}$. The NMR frequency being a function of the distribution of the magnetization $\vec{M}(\vec{r})$ over the whole sample, this gives nonlinear terms in the precession equations for $\vec{M}(\vec{r})$, which are the physical origin of the multiple echoes.

We can describe the effect of exchange and dipolar interactions on a microscopic range by effective equations which are the Bloch equations used in the high-temperature paramagnetic phase, i.e., with a transverse and longitudinal relaxation times T_2 and T_1 and a diffusion coefficient D

$$\frac{d\vec{M}(\vec{r})}{dt} = \gamma \vec{M}(\vec{r}) \times [\vec{H}(\vec{r}) + \vec{H}_d(\vec{r})] - \frac{M_z - M_0}{T_1}\vec{z} - \frac{M_x \vec{x} + M_y \vec{y}}{T_2} + D\nabla^2 \vec{M}(\vec{r}) \ . \tag{3}$$

In this equation, the field $\vec{H}(\vec{r})$ is taken parallel to $\vec{z}$ and M_0 is the equilibrium magnetization. We note that this model describes the behavior of our system to zero order in $\mathcal{H}/k_B T$ when high-temperature expansion is a valid approximation. The long-range demagnetizing field, proportional to $\vec{M}$, is used here to first order in $\gamma \hbar H S_z / k_B T$ and thus, in order to be consistent, we need to include into the microscopic effective equations the terms of order 1 in $\mathcal{H}_{ex}/k_B T$ and $\gamma \hbar H S_z / k_B T$. Apart from changes in T_1 and T_2, the most important effect of these terms is to change slightly the NMR frequency as function of the orientation of the magnetization with respect to crystal axis and external magnetic field. These terms contain $\mathcal{H}_d$ to first order; thus in bcc ^{3}He their anisotropic effect is zero because a second-order tensor such as $\mathcal{H}_d$ is isotropic in a cubic symmetry. Thus, in our experimental situation in bcc ^{3}He, the nonlinear anisotropic effect comes only from the local demagnetizing field. On the contrary, this is no longer true in hcp crystals where the NMR frequency is expected to be a function of the magnetization orientation with respect to the crystal axis; this change is estimated to be of the same order of magnitude as that produced by the long-range demagnetizing field. Consequently, although multiple echoes are also expected in hcp crystals, their quantitative behavior is not described by the theory presented in this paper.

We remark that at very low temperature, i.e., near or even below the spin ordering temperature, the intrinsic dipolar anisotropy on the microscopic scale can be larger than the demagnetizing effect in low field, especially in the hcp phase. In the spin ordered ^{3}He bcc phase, the microscopic anisotropy energy, of order $\mathcal{H}_D^2/\mathcal{H}_{ex}$, can be easily made smaller than the long-range demagnetizing energy $\mathcal{H}_D(\gamma \hbar H S_z/\mathcal{H}_{ex})$ when $H >> H_d$, i.e., $H >> 10$ G. Thus the assumptions of our theory of multiple echoes in bcc ^{3}He still hold below the ordering transition temperature ($T_c \sim 1$ mK) as soon as $H >> 10$ G. This remark proves that this theory can be used near the ordering temperature of bcc ^{3}He to measure the magnetic susceptibility of the solid, as explained in Sec. III.

Due to the nonlocal nature of $\vec{H}_d(\vec{r})$, Eq. (3) is very difficult to solve in general. Nevertheless, it can be significantly simplified if one can suppress the effect of the sample shape on the demagnetization distribution; this can be achieved by applying a strong uniform external field gradient G along the direction of a unit vector $\hat{s}$. Let us specify this important condition for the field gradient: at time $t = 0$, after the first rf pulse of angle α_1, the magnetization is uniform over the sample and thus the demagnetizing field $\vec{H}_d(\vec{r})$ is a function of both $\vec{r}$ and the shape of the sample. At $t > 0$, the magnetization has evolved following Eq. (3); if $t << T_1$ and T_2, the main term of the right-hand side of Eq. (3) is

$$\gamma \vec{M}(\vec{r})[\vec{H}(\vec{r}) + \vec{H}_d(\vec{r})] = \gamma \vec{M}(\vec{r})[\vec{H}_0 + G(\hat{s}\cdot\vec{r})\hat{s} + \vec{H}_d(\vec{r})]$$

Under the action of $\vec{H}(\vec{r})$ alone, the magnetization forms a spatial helix along the direction $\hat{s}$ with a pitch $2\pi/\gamma Gt$ decreasing with time. The free precession time $t_c = 2\pi/\gamma Gl$ is defined as the time at which the pitch of the helix is equal to the characteristic size l of the sample. During times of order t_c, the distribution of $\vec{H}_d(\vec{r})$ is very complex, due to the spatial distribution of the magnetization. Thus we make the important assumption that $H_d \sim 4\pi M_0$ is small enough not to disturb the formation of the helix by the gradient G or, equivalently, that H_d is negligible with respect to the magnetic field variation over the size l of the sample, i.e., $Gl >> H_d \sim 4\pi M_0$ or

$$4\pi M_0 \frac{1}{Gl} << 1 \quad . \tag{4}$$

With this condition, at times much larger than t_c, the helical magnetization over the sample produces a simple helical demagnetizing field as calculated in Sec. II B. The demagnetizing field effect (H_d of order $4\pi M_0$ is independent of time) becomes larger than the gradient effect when the magnetic field variation over the helix pitch $(2\pi/\gamma Gt)G$ is smaller than H_d, i.e., at times larger than t_e defined by

$$t_e \sim \frac{2\pi}{\gamma H_d} \sim \frac{1}{2\gamma M_0} \quad .$$

Thus, the demagnetizing field H_d is expected to have an important effect at times $t > t_e$ which must occur before the relaxation effects appearing in Eq. (3) reduce strongly the local transverse magnetization. Therefor $T_2 > t_e$, or

$$\gamma 4\pi M_0 T_2 > 2\pi \quad , \tag{5a}$$

is the condition for observing large multiple echoes. Actually, multiple echoes can be experimentally observed as soon as

$$\gamma 4\pi M_0 T_2 > 1 \quad . \tag{5b}$$

It is worth noting that conditions (4) and (5a) are independent. Following Eq. (5a), large multiple echoes can appear even if the condition (4) is not fulfilled. But in this case, the structure of the echo pattern is a very complex function of the shape of the sample so that the condition (4) is necessary in order to obtain well defined and useful results. Let us remark that the condition (4) can be always fulfilled by increasing the magnetic field gradient. A short analysis of the experimental results obtained when the condition (4) is not satisfied together with the explanation for the apparent very fast longitudinal relaxation of M_z then observed at short times, are given in Sec. III D.

In a first step, we derive simple analytical results neglecting the diffusion ($D = 0$). This can be seen as follows: we suppose that the spatial helix pitch remains large enough so that the diffusion time t_D over the pitch is much larger than the experimental time t, i.e., $t_D \sim [D(\gamma Gt)^2]^{-1} >> t$ or, as t is of the order of T_2

$$D\gamma^2 G^2 T_2^3 << 1 \quad . \tag{6}$$

The conditions (4) and (6) are not independent. Actually, the field gradients required to satisfy Eq. (4) often result in violation of condition (6). Thus in a second step, we present complete calculations including the diffusion effects; these are more complex than without diffusion and require numerical calculations; however they are much simpler than the calculations needed in the case of an unfulfilled condition (4) for which the very complicated results depend on the shape of the sample.

B. Relation between magnetization and demagnetizing field

Equation (2) relates the magnetization $\vec{M}(\vec{r})$ and the demagnetizing field $\vec{H}_d(\vec{r})$. As $H_0 >> H_d$, we can neglect the demagnetizing field components at frequencies $\Omega_0 = \gamma H_0 >> \gamma H_d \sim \gamma 4\pi M_0$; this is done by taking only into account the secular part of $\mathcal{H}_D$ which is invariant with respect to a rotation around $\vec{H}_0$.[21] We get the usual expression of the dipolar field

$$\vec{H}_d(\vec{r}) = \int d^3r' \frac{1 - 3\cos^2\theta_{rr'}}{2|\vec{r} - \vec{r}'|^3} \times [3M_z(\vec{r}')\hat{z} - \vec{M}(\vec{r}')] \quad , \tag{7}$$

where $\hat{z}$ is the unit vector parallel to $\vec{H}_0$ and $\theta_{rr'}$ is the angle between $(\vec{r} - \vec{r}')$ and $\hat{z}$.

This nonlocal relation becomes simpler and local after a Fourier transformation of $\vec{H}_d(\vec{r})$ and $\vec{M}(\vec{r})$

$$\vec{H}_d(\vec{k}) = \int d^3r \, e^{i\vec{k}\cdot\vec{r}} \vec{H}_d(\vec{r}) \quad ,$$

$$\vec{M}(\vec{k}) = \int d^3r \, e^{i\vec{k}\cdot\vec{r}} \vec{M}(\vec{r}) \quad .$$

We find[20]

$$\vec{H}_d(\vec{k}) = \tfrac{1}{3}(4\pi)\tfrac{1}{2}[1 - 3(\hat{k}\cdot\hat{z})^2] \times [\vec{M}(\vec{k}) - 3M_z(\vec{k})\hat{z}] = \underline{C}_{\vec{k}} \vec{M}(\vec{k}) \quad , \tag{8}$$

where $\hat{k} = \vec{k}/|\vec{k}|$.

We note that the tensor $\underline{C}_{\vec{k}}$ is a function of the orientation of vector $\vec{k}$ and not of $|\vec{k}|$. Thus, if the magnetization $\vec{M}(\vec{r})$ is a function only of the one-dimensional variation $\hat{s}\cdot\vec{r} = s$, i.e., if it has nonzero Fourier components only for $\vec{k}$ parallel to $\vec{s}$, we have again, in the real space, a simple local relation between $\vec{H}_d(\vec{r})$ and $\vec{M}(\vec{r})$ instead of the complex relation (7)

$$\vec{H}_d(\vec{r}) = \underline{C}_{\hat{s}} \cdot \vec{M}(\vec{r}) = \vec{H}_d(s) \quad . \tag{9}$$

Furthermore, we see that if at some time t_0, $\vec{M}(\vec{r})$ is one dimensional (which means that it is a function only of $s=\hat{s}\cdot\vec{r}$), the evolution equation (3) shows that it remains one dimensional at later times $t>t_0$, as only the one variable terms $\vec{M}(s)$ and $\partial^2\vec{M}(s)/\partial s^2$ appear in this equation. Now, we saw in Sec. II A that at times $t>t_c=2\pi/\gamma Gl$, the magnetization $\vec{M}(\vec{r})$ in the sample is a helix along the direction $\hat{s}$ and so is a one-dimensional function of s. Thus at later times, although $\vec{M}(\vec{r})$ is no longer a simple helix under the action of $\vec{H}_d(s)$, it remains a function of s only, so that the relation (9) can be used exactly in Eq. (3). To do that is equivalent to neglecting edge effects of the sample: this is a very good approximation in as much as condition (4) is fulfilled. Thus, later on we shall take $\vec{M}(\hat{s})=\vec{M}(s)$ to be a function of the one-dimensional variable s.

The relation (9) can be rewritten

$$\vec{H}_d(s)=\underline{C}_s\cdot\vec{M}(s)=\beta M_z(s)\hat{z}-\tfrac{1}{3}\beta\vec{M}(s)\ ,$$

with

$$\beta=2\pi[3(\hat{s}\cdot\hat{z})^2-1]\ .$$

This means that $\vec{H}_d(s)$ produces only a change in the NMR precession frequency

$$\delta\Omega=\gamma\beta M_z(s)\ , \tag{10}$$

as the transverse component of $\vec{H}_d(s)$, parallel to $\vec{M}(s)$, does not affect the precession of $\vec{M}(s)$. Thus the apparent effect of $\vec{H}_d(r)$ is identical to a change in the local external field. If $\vec{M}(\vec{r})$ were not one dimensional, the precession of $\vec{M}(\vec{r})$ around $\vec{H}_d(\vec{r})$ would give not only a change in the precession frequency but also a change of $M_z(\vec{r})$ with time, an effect which is discussed in Sec. III D.

C. Theory of multiple echoes neglecting diffusion

Just after the application of a rf pulse of angle α_1 at time 0, we have the following equations:

$$\left.\begin{aligned} &M_z(0^+)=M_0\cos\alpha_1\ ,\\ &M^{\pm}(0^+)=\mp iM_0\sin\alpha_1=M_x\pm iM_y\end{aligned}\right\}\ . \tag{11}$$

After the pulse, M_z remains spatially uniform and there is no particular effect of the demagnetizing field during times between 0 and τ, except for a negligible change of the free precession frequency $\delta\Omega=\gamma\beta M_z(0_+)$, which can be included in the external field. The truncated Eq. (3) ($D=0$) gives

$$\frac{dM_z}{dt}=-\frac{1}{T_1}(M_z-M_0)\ ,$$

$$\frac{dM^+}{dt}=i\gamma(H_0+Gs)M^+ +i\gamma\beta M_zM^+-\frac{1}{T_2}M^+\ .$$

The solutions of these equations for $t<\tau$ are

$$\begin{aligned} M_z(t)&=M_0[1+(\cos\alpha_1-1)e^{-t/T_1}]\ ,\\ M^+(t)&=-iM_0\sin\alpha_1 e^{i\gamma(Gs+H_0)t}\\ &\quad\times e^{-t/T_2}\exp\left[i\beta\gamma\int_0^t M_z(t')\,dt'\right]\ .\end{aligned} \tag{12}$$

The last term in the $M^+(t)$ expression shows that the phase of the local magnetization is changed proportionally to the time integral of the longitudinal magnetization M_z. Just before the second pulse, at time τ^-, the magnetization has a helical distribution over the sample given by

$$\begin{aligned} &M_z(\tau^-)=M_0[1+(\cos\alpha_1-1)e^{-\tau/T_1}]\ ,\\ &M^+(\tau^-)=-iM_0\sin\alpha_1 e^{i\gamma H_0\tau}e^{ik_0s}e^{-\tau/T_2}\exp\{i\beta M_0\gamma[\tau-T_1(e^{-\tau/T_1}-1)(\cos\alpha_1-1)]\}\ ,\end{aligned} \tag{13}$$

where we have introduced the wave number $k_0=\gamma G\tau$.

The second rf pulse at time τ rotates the magnetization by an angle α_2 around the radio-frequency field $\vec{H}_1$, so that the helical structure is converted into a sinusoidal modulation of the magnetization along the gradient direction $\hat{s}$. Just after the second pulse, we have

$$M_z(\tau^+)=M_z(\tau^-)\cos\alpha_2+\frac{M^+(\tau^-)-M^-(\tau^-)}{2i}\sin\alpha_2$$

$$M^+(\tau^+)=-iM_z(\tau^-)\sin\alpha_2+\frac{M^+(\tau^-)}{2}(1+\cos\alpha_2)$$

$$+\tfrac{1}{2}[M^-(\tau^-)](1-\cos\alpha_2)\ .$$

This can be written in a compact form emphasizing the spatial variations

$$\begin{aligned} &M_z(\tau^+)=[A+B\sin(\Omega_0\tau+k_0s+\phi_0)]M_0\ ,\\ &M^+(\tau^+)=(C-D^+e^{ik_0s}+D^-e^{-ik_0s})M_0\ ,\end{aligned} \tag{14}$$

with

$$A=\cos\alpha_2[1+(\cos\alpha_1-1)e^{-\tau/T_2}]\ ,$$

$$B=\sin\alpha_1\sin\alpha_2 e^{-\tau/T_2}\ ,$$

$$\phi_0=\gamma\beta M_0[\tau-(\cos\alpha_1-1)T_1(e^{-\tau/T_1}-1)]\ ,$$

$$C=-iA\,\mathrm{tg}\,\alpha_2\ ,$$

$$D^{\pm}=\tfrac{1}{2}i(1\pm\cos\alpha_2)\sin\alpha_1 e^{-\tau/T_2}e^{i\phi_0}\ .$$

The demagnetizing field corresponding to $M_z(\tau^+)$ generates a spatially sinusoidally modulated Larmor frequency which acts on the transverse M^+ helix as it did before the second pulse so that the expression of $M^+(t)$ in Eq. (12) remains valid if we use the correct initial values and time evolution, i.e., $M^+(\tau^+)$ replacing M_0 and τ being the initial time instead of 0. We find

$$M^+(t) = M^+(\tau^+) e^{i\gamma[H_0+Gs(t-\tau)]} e^{-(t-\tau)/T_2} \exp\left\{ i\gamma\beta M_0 \left[(t-\tau) - \left(\frac{M_z(\tau^+)-1}{M_0} \right) T_1 (e^{-(t-\tau)/T_1} - 1) \right] \right\} .$$

Making explicit only the gradient dependent terms of this equation, we obtain

$$M^+(t) = (C - D^+ e^{ik_0 s} + D^- e^{-ik_0 s}) E e^{ik_0 s[(t/\tau)-1]} e^{i\delta(t)\sin(k_0 s+\phi_0)} ,$$

with

$$\delta(t) = \delta_t = \gamma\beta M_0 \sin\alpha_1 \sin\alpha_2 T_1 e^{-(t/T_2)} (1 - e^{(t-\tau)/T_1}) , \quad E = M_0 e^{-t/T_2} \exp i\gamma\beta M_0 [t + T_1 (e^{-(t-\tau)/T_1} - 1)(1 - A)] . \tag{15}$$

As for conventional NMR echoes, we experimentally measure the uniform part of the magnetization $M^+(t)$, i.e., the spatial Fourier component $k = 0$.

Using the Bessel-function expansion

$$e^{i\delta\sin(k_0 s+\phi_0)} = \sum_{-\infty}^{\infty} J_n(\delta) \exp[in(k_0 s + \phi_0)]$$

we can obtain the different Fourier components of $M^+(t)$.

At time $t = p\tau$ with integer $p \geq 2$, the amplitude of the echoes is given by the Fourier component of $k = 0$, i.e., a combination of Bessel functions with $n = 1-p$, $n = 1-p+1$, and $n = 1-p-1$

$$A_p = C e^{i(1-p)\phi_0} J_{1-p}(\delta_{p\tau}) - D^+ e^{-ip\phi_0} J_{-p}(\delta_{p\tau}) + D^- e^{i(2-p)\phi_0} J_{2-p}(\delta_{p\tau}) ,$$

which gives

$$|A_p| = M_0 e^{-(p\tau/T_2)} \left| \sin\alpha_1 \left(\frac{1+\cos\alpha_2}{2} \right) J_p(\delta_{p\tau}) + \sin\alpha_1 \left(\frac{1-\cos\alpha_2}{2} \right) J_{p-2}(\delta_{p\tau}) \right.$$
$$\left. + i \sin\alpha_2 [1 + (\cos\alpha_1 - 1) e^{-(\tau/T_1)}] e^{-(\tau/T_2)} J_{p-1}(\delta_{p\tau}) \right| .$$

With two 90° pulses ($\alpha_1 = \alpha_2 = 90°$) the expression simplifies, by virtue of

$$J_p(\delta) + J_{p-2}(\delta) = \frac{2(p-1)}{\delta} J_{p-1}(\delta) ,$$

to

$$|A_p| = e^{-(p\tau/T_2)} \left| \frac{p-1}{\delta_{p\tau}} + i(1 - e^{-(\tau/T_1)}) e^{-(\tau/T_2)} \right| J_{p-1}(\delta_{p\tau}) . \tag{16}$$

The amplitude of a given echo at time $p\tau$ oscillates like $|J_{p-1}(\delta_{p\tau})|$ with perfectly well defined zeroes which are damped for values of α_1 or α_2 different from 90°. If there is no demagnetizing field, i.e., if $\beta M_0 = 0$, we find the usual single echo at $t = 2\tau$. As βM_0 increases, multiple echoes appear; for small values of βM_0, their amplitudes are given by expansion of the Bessel functions

$$A_p \simeq e^{-(p\tau/T_2)} \sin\alpha_1 \left(\frac{1-\cos\alpha_2}{2} \right) \times \left(\frac{\delta_{p\tau}}{2} \right)^{p-2} \frac{1}{(p-2)!} \quad \text{for } p \geq 3 .$$

The characteristic parameter which governs the echo pattern is $b = \gamma\beta M_0 T_2$; the multiple echoes become easily detectable as soon as $b \geq 1$. For two 90° rf pulses, the echo amplitudes exhibit zero values when b is greater than 11 (the exact b value is a function of the ratio T_1/T_2) as can be seen from the expression (15) giving the argument $\delta(t)$ of the Bessel functions: if T_1 and T_2 are very short, as t increases this argument remains smaller than the value corresponding to the first zero of the Bessel function.

In order to satisfy the important condition (4), it is often necessary to use a large field gradient and consequently the diffusion effect can no longer be neglected. It is for this reason that we shall now calculate the multiple echo amplitudes when taking into account self-diffusion.

D. Theory of multiple echoes in presence of diffusion

The diffusion term of Eq. (3), $D\partial^2\vec{M}/\partial s^2$, damps the spatial variation of $\vec{M}$ so that an analytical expression of multiple-echo amplitudes cannot be obtained. A perturbation theory becomes rapidly invalid as the parameter $d = D\gamma^2G^2t^3$, which measures the strength of the diffusion effect, is larger than 0.1, especially near the minima of the echoes. A numerical calculation is then necessary.

Let us recall that the essential assumption prescribing that $\vec{M}(\vec{r})$ is only function of the one-dimensional variable s remains valid even in the presence of diffusion. The equations to be solved are

$$\left.\begin{aligned} \frac{dM_z}{dt} &= -\frac{1}{T_1}(M_z - M_0) + D\nabla^2 M_z \\ \frac{dM^+}{dt} &= i\gamma(H_0 + Gs)M^+ - \frac{1}{T_2}M^+ \\ &\quad + i\gamma\beta M_z M^+ + D\nabla^2 M^+ \end{aligned}\right\} . \qquad (17)$$

We make a spatial Fourier analysis of M_z and M^+

$$\vec{M}_k = \int \vec{M}(s)e^{iks}\,ds ,$$

which gives for M_z

$$\frac{dM_{zk}}{dt} = -\left(\frac{1}{T_1} + Dk^2\right)M_{zk} ,$$

so that each Fourier component of M^+ relaxes with an apparent relaxation time

$$T_{1k}^{*-1} = T_1^{-1} + Dk^2 .$$

On the other hand, the transverse component M^+ equation remains complicated because the demagnetizing field product $\beta M_z(s)M^+(s)$ becomes a convolution integral after Fourier transformation. However, before the second pulse ($0 \leq t < \tau$), $M_z(s)$ is spatially uniform so that the equations of evolution of M_z and M^+, nonaffected by the demagnetizing field, are the same as usual[21] with only the classical diffusion effect for M^+. At time τ^- we obtain

$$M_z(\tau^-) = M_0[1 + (\cos\alpha_1 - 1)e^{-\tau/T_1}] ,$$

$$M^+(\tau^-) = -iM_0 \sin\alpha_1 e^{-\tau/T_2^*} e^{i\phi_0} e^{i(\gamma H_0\tau + k_0 s)} ,$$

with

$$T_2^{*-1} = T_2^{-1} + \tfrac{1}{3}D\gamma^2G^2\tau^2 .$$

Thus, formula (14) of Sec. II C giving $\vec{M}(\tau^+)$ after the second pulse remains valid if we replace T_2 by T_2^* in order to take into account the diffusion at times before τ^+. We need now to solve Eq. (17) for times greater than τ^+. As noted above, we take into account the diffusion for each Fourier component of $M_z(t)$ by replacing T_1 by T_{1k}^*. For $M^+(t)$, this simple procedure is not possible as, under the action of the field gradient, the k values change linearly with time. It is convenient, before Fourier transformation, to make the substitution

$$M^+(s) = S^+(s)e^{i\gamma Gs(t-\tau)} = S^+(s)e^{ik_0 s(t/\tau - 1)} ,$$

which gives

$$\frac{dS^+(s)}{dt} = i\omega(s)S^+(s) + D\left[\frac{\partial^2 S^+(s)}{\partial s^2} + 2i\gamma G(t-\tau)\frac{\partial S^+(s)}{\partial s} - \gamma^2G^2(t-\tau)^2S^+(s)\right] ,$$

with

$$\omega(s) = \gamma(H_0 + \beta M_z) + i/T_2 . \qquad (18)$$

Then, after Fourier transform of $S^+(s)$ and $\omega(s)$

$$S_k^+ = \int S^+(s)e^{iks}\,ds , \qquad \omega_k = \int \omega(s)e^{iks}\,ds ,$$

we obtain

$$\frac{dS_k^+}{dt} = \int i\omega_{k_1}S_{k-k_1}^+\,dk_1 - D[k + \gamma G(t-\tau)]^2 S_k^+ . \qquad (19)$$

At $t=\tau$ [initial time for Eq. (19)], we have only three nonzero Fourier components for $k=0$ and $k=\pm k_0$ [see Eq. (14)]. Thus in Eq. (19), we have only nonzero components for k multiple of k_0: $k=pk_0$, p integer <0, or ≥ 0. The expressions of the three Fourier components of $\omega(s)$ for every time $t \geq \tau$ are

$$\omega_0 = \gamma H_0 + \frac{i}{T_2} + \gamma\beta M_0[1 + (\cos\alpha_2 - 1)e^{-(t-\tau)/T_1} + \cos\alpha_2(\cos\alpha_1 - 1)e^{-t/T_2}] ,$$

$$\omega_{k_0} = -\tfrac{1}{2}(\gamma\beta M_0)\sin\alpha_1 \sin\alpha_2 e^{-\tau/T_2} e^{-(t-\tau)/(T_{1k_0}^*)} = \omega_{-k_0} .$$

In the same way, the three Fourier components of $S_k(\tau^+)$ are

$$S_0^+(\tau^+) = -iM_0 \sin\alpha_2[1 + (\cos\alpha_1 - 1)e^{-\tau/T_2}] ,$$

$$S_{\pm k_0}^+(\tau^+) = \mp iM_0 \sin\alpha_1(1 \pm \cos\alpha_2)e^{-\tau/T_2^*} .$$

Without demagnetizing field effects, Eq. (19) reduces to the usual simple equation including the diffusion ($\omega_{k_1} = \omega_0 \delta_{k_1,0}$) in which each component evolves independently of the others. In order to suppress this trivial evolution, we make the transformation

$$S_k^+(t) = U_k(t) e^{if(t)} e^{i\Phi_k(t)} ,$$

with

$$f(t) = \int_\tau^t \omega_0(t')\, dt' ,$$

$$\phi_k(t) = -D\int_\tau^t [k + \gamma G(t' - \tau)]^2\, dt' .$$

The equation of motion for $U_k(t)$ is

$$\frac{dU_k(t)}{dt} = \sum_{k_1} i\omega_{k-k_1}(t)\, U_{k_1}(t)\, e^{(\Phi_{k_1} - \Phi_k)} , \qquad (20)$$

with

$$k - k_1 = \pm k_0 \text{ and } k_1 = pk_0 .$$

Starting from the initial conditions $\omega_k(\tau^+)$ and $U_k(\tau^+)$, we have calculated on a computer the components U_k as a function of time, using a Runge-Kutta[22] integration method. The stability of the solution has been satisfactorily tested by varying the width of the integration time step and the number of the Fourier components (of the order of 60). We made a further precise test by calculating with this method the echo amplitudes when $D=0$ and we found again, with a good accuracy, the values obtained using the analytical Bessel functions solutions. The amplitude of the echo of order $(p-1)$ at time $p\tau$ is given by the component of $M_k(p\tau)$ at $k=0$, i.e., by $S_{(p-1)k_0}(p\tau)$. The results of this calculation are postponed to Sec. III in order to compare them directly with the experimental results.

III. EXPERIMENTAL RESULTS

We already mentioned that solid ^{3}He was a good candidate for the study of multiple echoes, owing to the following interesting properties: large gyromagnetic ratio γ giving a large dipolar magnetic field, large transverse relaxation time T_2 due to the "motional narrowing of the line" and hence large value of the coefficient $b=\gamma\beta M_0 T_2$ which mainly governs the behavior of the echoes, facility of varying the molar volume and hence T_2, and the diffusion coefficient D. Furthermore, this solid can be studied over a very large temperature range as illustrated by the two sets of experiments analyzed in this paper; one set performed at temperatures between 750 and 300 mK we call the "high-temperature" experiments and the other performed between 20 and 1 mK, we call the "low-temperature" experiments.

A. Experimental situation

1. *Low-temperature experiments*

In the low-temperature and low-field experiments ($19 < H_0 < 77$ G) the solid ^{3}He sample was formed in a Pomeranchuk cell and consequently was in contact with liquid ^{3}He along the melting curve at a molar volume of about 24.25 cm^3. Both the main magnetic field H_0 and the gradient G were produced by the same large dimension Helmoltz coil pair and hence both H_0 and G were uniform over the whole sample. With these conditions, reproducible multiple-echo patterns were easily obtained.

2. *High-temperature experiments*

On the other hand, some experimental difficulties were encountered in the high-temperature experiments, which will be described below. We made this set of experiments in order to test the validity of the theory in a region where the magnetic properties of ^{3}He are well known, without low-temperature (or

pretransitional) effects. In the half degree temperature range, where we needed a high magnetic field, we used $H_0 = 9250$ G produced by a conventional 9 in. Varian electromagnet. This rather high value of H_0 had some important consequences:

(i) With such a field, the intrinsic inhomogeneity of the magnet is of the order of 0.2 G cm^{-1}; thus in order to obtain a rather well defined linear field gradient, the applied external field gradient must be larger than 1 G cm^{-1}. We produced it by a set of two coils in Maxwell positions attached to the external bottom end of the cryostat and we controlled its amplitude by varying the current in the coils.

(ii) In such large gradients, the rf field H_1 is not much greater than the static field variation $\Delta H = Gl$ along the length l of the sample; thus the rotation angle α of the magnetization due to the rf pulse is not homogeneous in the whole sample. For instance with $H_1 = 13$ G, $l = 0.6$ cm, and $G = 7$ G cm^{-1}, the maximal dispersion of α during a rf pulse is of the order of $\frac{1}{20}\pi$ [this means that a $\frac{1}{2}\pi$ pulse is actually seen as a pulse ranging from $\frac{1}{20}(9\pi)$ to $\frac{1}{20}(11\pi)$, according to the location of the spin in the sample]. Fortunately, this dispersion of tipping angle has only a small effect on the amplitudes of the minima of the echoes and has no effect—to first order—on their positions, as we verified by computing the echoes amplitudes with various pulse angles.

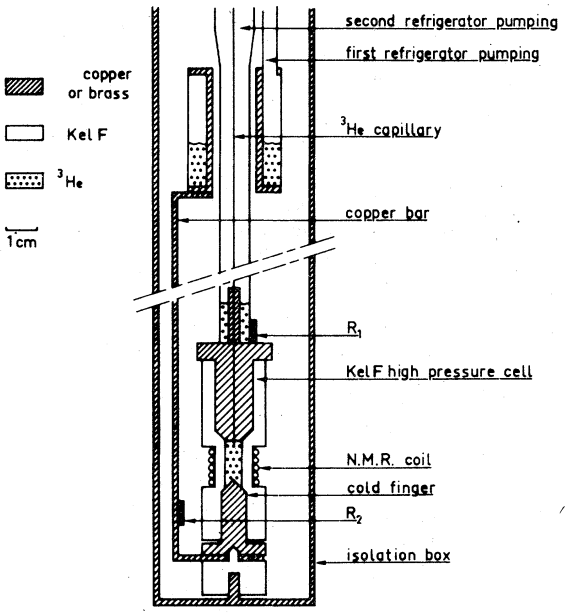

FIG. 1. Schematic view of the cell and of the two ^{3}He refrigerators. R_1 and R_2 are carbon resistors thermometers. The blocking of the ^{3}He capillary is prevented by maintaining its temperature slightly above the melting temperature by thermal contact with the second pumped ^{3}He refrigerator. The bottom of the cell is cooled down by the cold finger in thermal contact with the first ^{3}He refrigerator.

(iii) Vibrations of the sample in a field gradient generate field fluctuations which may modify strongly the echo pattern if the fluctuations amplitudes are equal or larger than the sample magnetization. With $H_0 = 9250$ G and $T = 500$ mK, the internal field is of the order of 5 mG, corresponding to a vibration amplitude of 10^{-3} cm in a 5 G cm^{-1} field gradient. Thus, the high-pressure sample cell must be tightly connected to the other parts of the cryostat. In our experiment, this mechanical brace leads to some thermal loss which accounts for the poor minimal temperature ($T_{min} = 315$ mK) obtained for our one-shot ^{3}He refrigerator.

(iv) Both theoretical calculations[23] and experimental data[24] show an increasing anisotropy of the transverse and longitudinal relaxation times T_2 and T_1 with increasing external magnetic field H_0. In the 38.6 G average magnetic field used in the low-temperature experiments and with a 24.25 cm^3 molar volume samples, T_1 and T_2 are isotropic, owing to the large ratio Ω_e/Ω_0 of the exchange frequency of the solid Ω_e to the experimental Larmor frequency Ω_0. On the other hand, the anisotropic effect is expected to be large in a 9250 G magnetic field. Consequently, in samples made of several monocrystals randomly oriented, as they are produced by the "blocked capillary" growing method,[25,26] very complicated echo patterns are expected inasmuch as the evolution equations for $\vec{M}$ [see Eq. (17)] which depend on T_1 and T_2, are different for each monocrystal. For this reason, we must use a constant pressure growing method which is known to produce rather good monocrystalline samples.[24,27–29] Our constant pressure cell together with the refrigerators are shown on Fig. 1. During the solidification, the bottom of the cell is cooled with a cold copper finger thermally linked to a pumped ^{3}He refrigerator while the blocking of the capillary is prevented by maintaining its temperature slightly above the melting temperature by thermal contact with another pumped ^{3}He refrigerator. The capillary then allows liquid ^{3}He to flow freely so that the solid grows at constant pressure with a well defined solid-liquid interface. We did not perform a systematic study of the quality of our crystals and thus we cannot be sure that we always obtained good single crystals. Nevertheless, the rather well pronounced minima of the experimental echo amplitudes may be a good indication that our samples were monocrystalline.

B. Analysis of the high-temperature data

Among the large number of data that we obtained, we report in this section two sets of representative results: (i) With a given sample placed in a fixed field gradient, we report the multiple echoes measured at four temperatures between 750 and 315 mK with the

corresponding calculated amplitudes, and (ii) At fixed temperature, multiple echoes are measured in a sample placed in three different field gradients, emphasizing the diffusion effect.

Figures 2(a) and 2(b) represent typical multiple-echo patterns following sequences of two 90° pulses with different spacing times τ. It is worth noting that more than 30 echoes can be detected and that the echo amplitudes behavior can be strongly nonmonotonic, as shown in Fig. 2(b). The set of Figs. 3–6 shows:

(a) [Figs. 3(a) to 6(a)], the amplitude of the four echoes appearing at times $2\tau, 3\tau, 4\tau, 5\tau$, measured at four temperatures, and obtained with the same sample (molar volume =23 cm^3) placed in the same field gradient $G = 3$ G cm^{-1}. The amplitudes are normalized with the height of the free precession signal following a 90° pulse after complete recovery.

(b) [Figs. 3(b) to 6(b)], the calculated amplitudes obtained as explained in Sec. II D when taking into account the diffusion. T_1 is experimentally obtained through the recovery of the free precession signal after the second 90° pulse. T_2, D, and $b = \gamma\beta M_0 T_2$ are introduced as parameters in the computer calculation. For each temperature, T_2 is used as time unit in the time scale of all the figures (a) and (b).

The resulting values of T_1, T_2, D, and b are collected in Table I. We also calculated the ratio of the

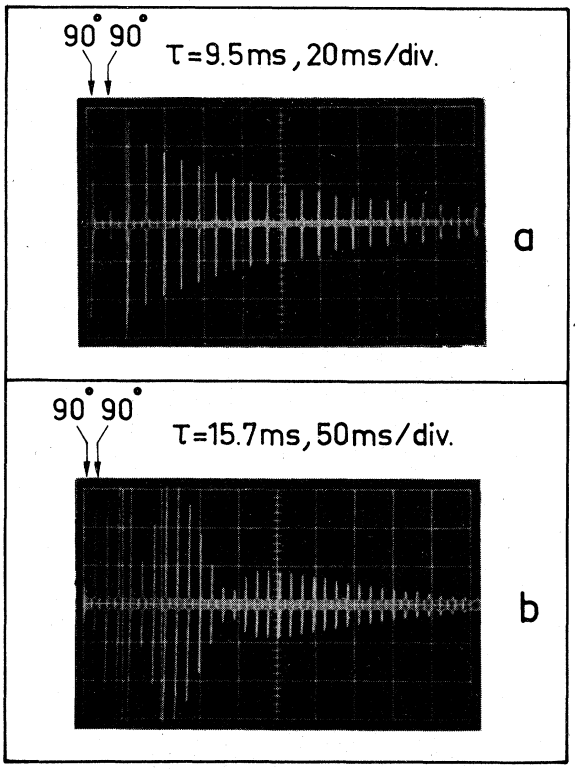

FIG. 2. Photographs of typical multiple echo patterns obtained for two values of the time interval τ between the 90° radio-frequency pulses. The temperature was $T = 320$ mK, the magnetic field was $H_0 = 9250$ G and the molar volume was $V_m = 23.6$ cm^3. At $\tau = 9.5$ msec, there is no minimum amplitude for any echo. At $\tau = 15.7$ msec, the echoes 4 and 12 reach their first and second minimal amplitude, respectively, so that the behavior of the whole pattern is strongly nonmonotonic. Owing to the strong field gradient, the free precession following the two pulses are narrow, thus the recovery time of the receiver prevents the observation of their early decay. Consequently, the observed free precession appearing in these photographs are not scaled with the echoes. Compared with Fig. 2(a), the gain is multiplied by 7 in Fig. 2(b).

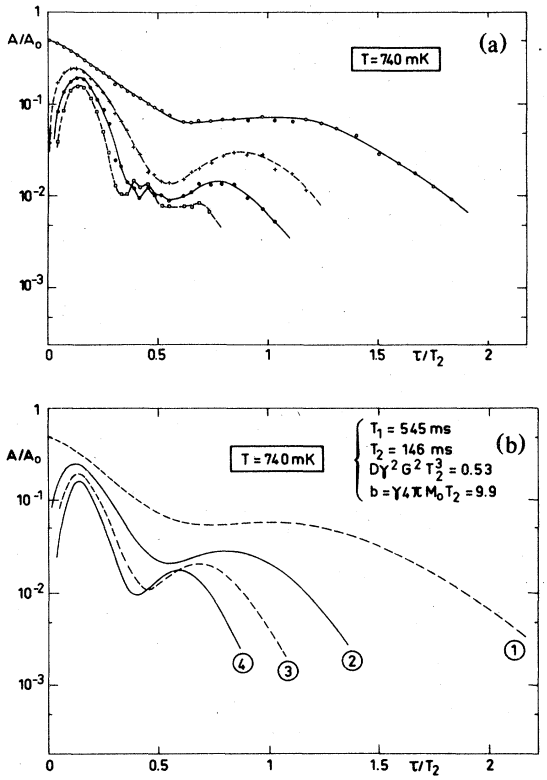

FIG. 3. Experimental (a) and calculated (b) amplitudes of some multiple echoes. The measurements were made at 740 mK with a sample of molar volume $V_m = 23$ cm^3 placed in a magnetic field $H_0 = 9250$ G ($\Omega_0/2\pi = 300$ MHz) and in a field gradient $G = 3$ G cm^{-1}. In this figure as in the Figs. 4, 5, and 6, for the sake of clarity only four or five echoes are reported though more than 40 echoes could be observed. For every experimental figure the continuous lines drawn through the data are only given as interpolation lines. The amplitude calculations were made as explained in the text, taking into account both the demagnetizing field effect and the diffusion effect.

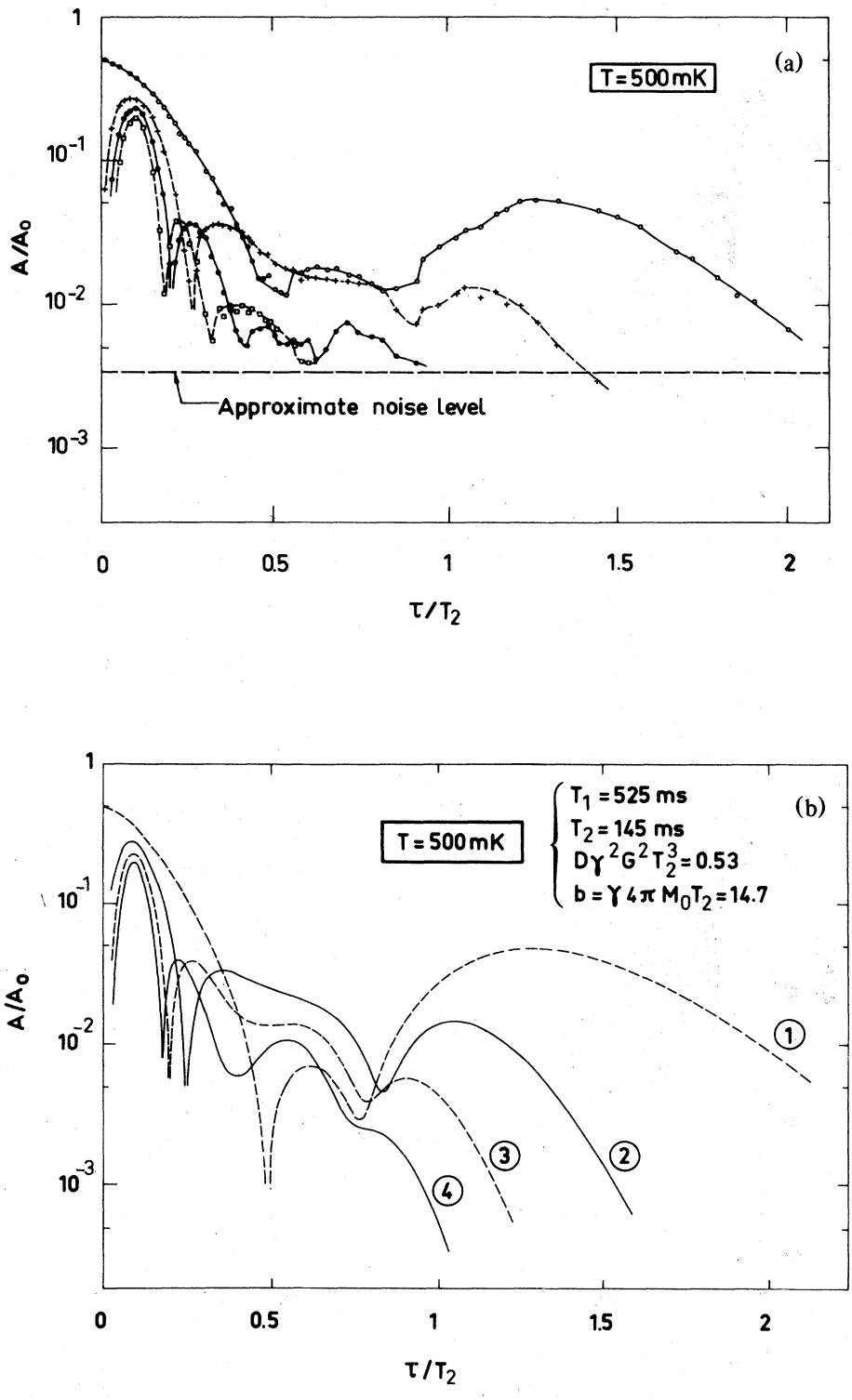

FIG. 4. Experimental (a) and calculated (b) amplitudes of some multiple echoes obtained under the same conditions as those described in Fig. 3, excepted the temperature which was $T = 500$ mK.

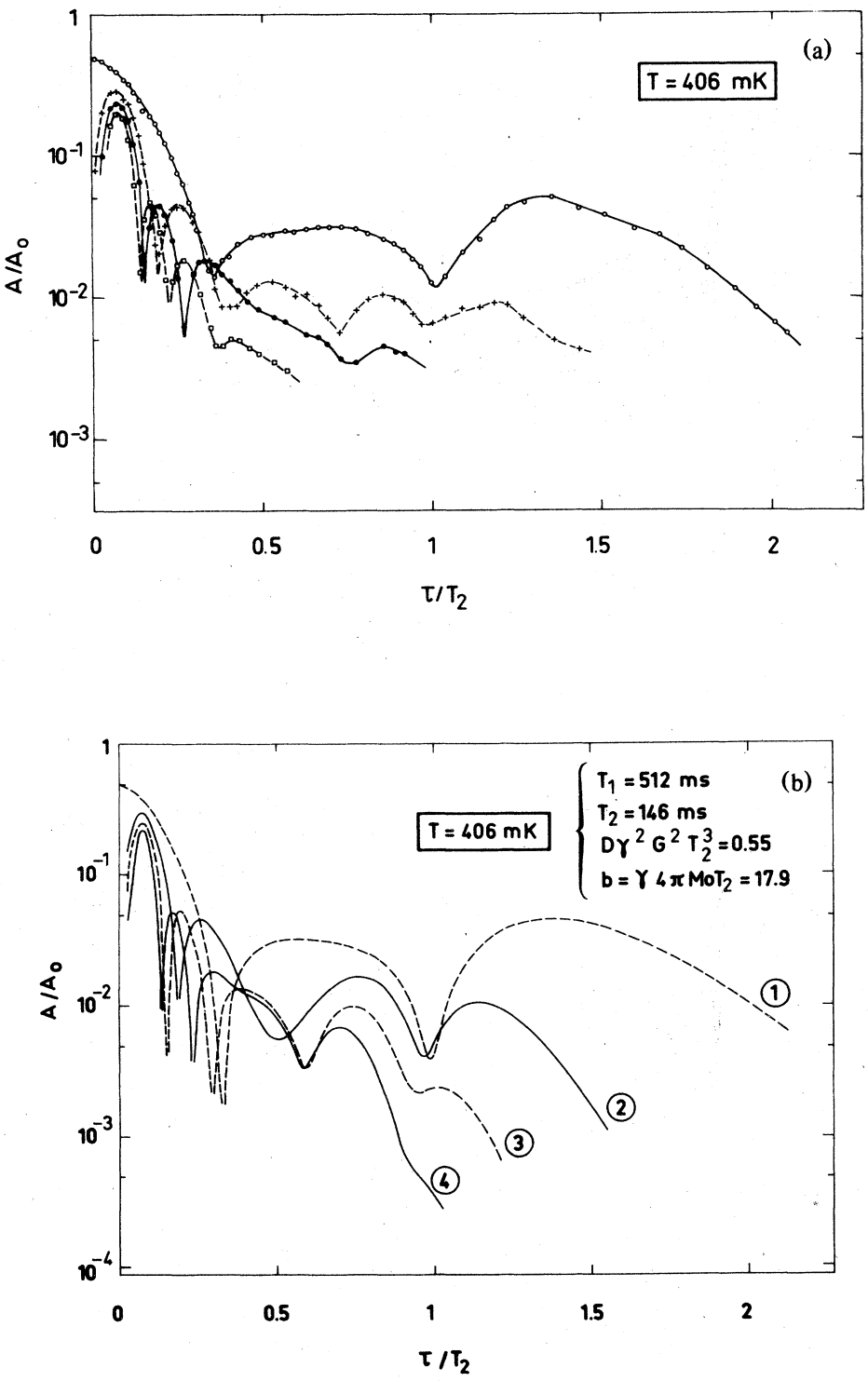

FIG. 5. Experimental (a) and calculated (b) amplitudes of some multiple echoes obtained under the same conditions as those described in Fig. 3, excepted the temperature which was $T = 406$ mK.

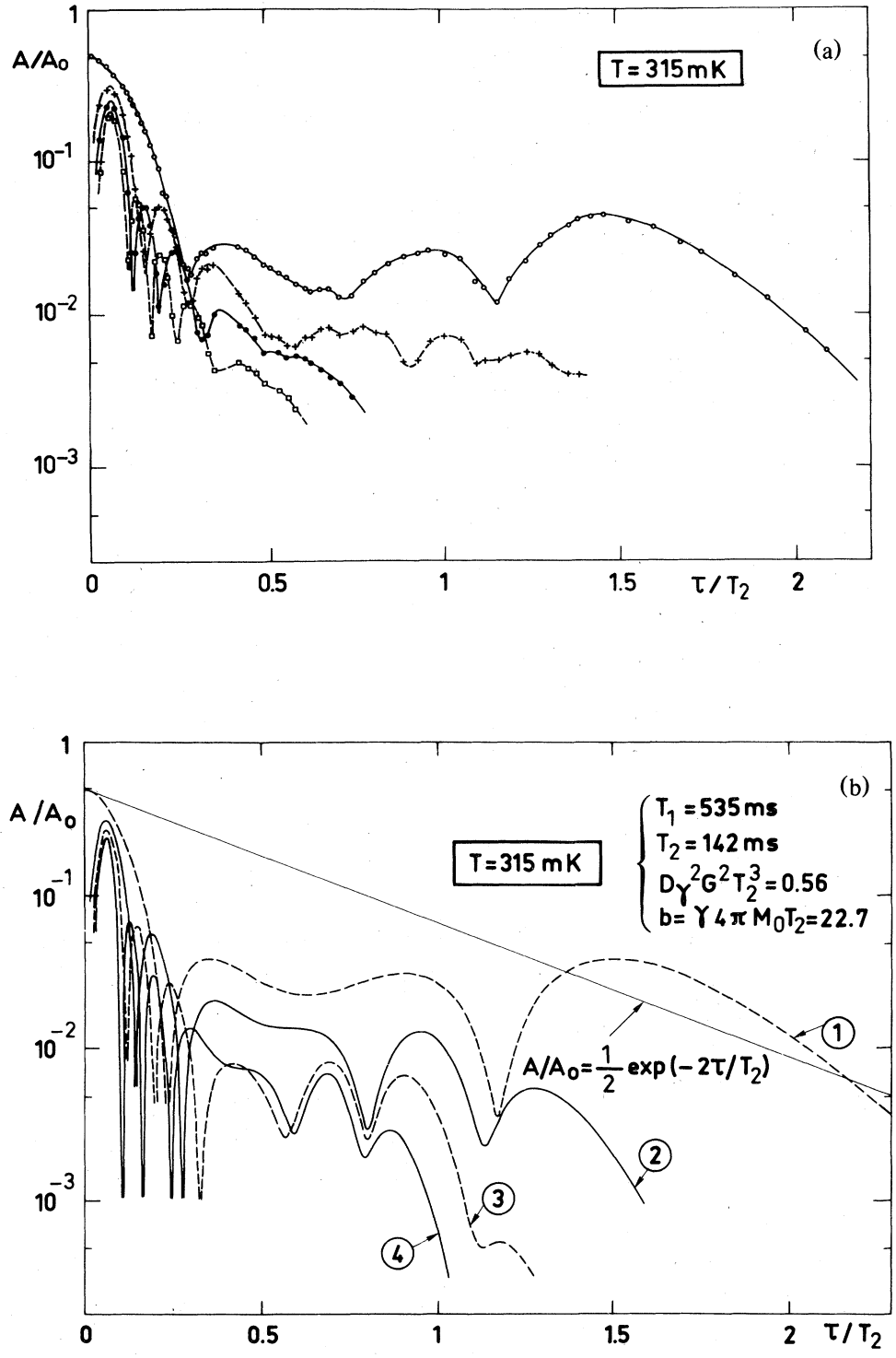

FIG. 6. Experimental (a) and calculated (b) amplitudes of some multiple echoes obtained under the same conditions as those described in Fig. 3, excepted the temperature which was $T=315$ mK. As an example we have reported on (b) the expected amplitude of the first echo when neither demagnetizing field nor diffusion occurs, i.e., $A/A_0=\frac{1}{2}\exp(-2\tau/T_2)$. This comparison emphasizes the amplification of the first echo due to the demagnetizing field, which appears here in the time interval $1.3T_2<\tau<2.2T_2$.

TABLE I. Longitudinal and transverse relaxation times T_1 and T_2, diffusion coefficient D, and magnetic susceptibility χ of a given sample, as determined by the analysis of the data reported in Figs. 3–6. The calculated magnetic susceptibility was obtained using $\chi_{calc} = [NI(I+1)\gamma^2\hbar^2/3k_BT]$, where N is the number of spins per unit volume. The experimental susceptibility was obtained using a demagnetizing coefficient β equal to 4π. The variations of the parameter b proportional to the magnetization M_0 govern the variations of the echo pattern with the temperature.

			^{3}He $V_m = 23$ cm^3		
T (mK)	T_1 (msec)	T_2 (msec)	$b = \gamma 4\pi M_0 T_2$	$\frac{\chi_{measured}}{\chi_{calculated}}$	D (10^{-8} cm^2 sec^{-1})
740	545	146	9.9	0.97	4.6
500	525	145	14.7	0.98	4.7
406	512	146	17.9	0.96	4.7
315	535	142	22.7	0.98	5.2

theoretical value of the magnetic susceptibility

$$\chi = [NI(I+1)\gamma^2\hbar^2/3k_BT] \ ,$$

where N is the number of spins per unit volume,

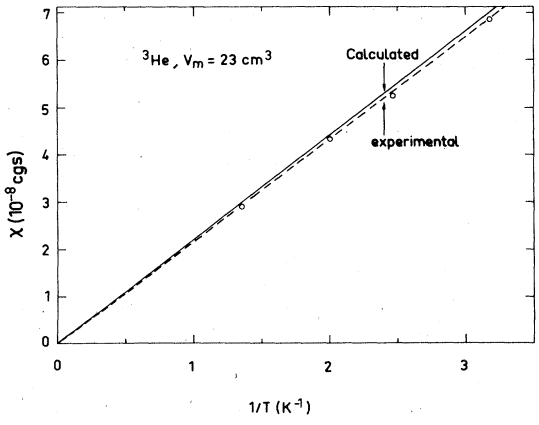

FIG. 7. Magnetic susceptibility χ solid ^{3}He, $V_m = 23$ cm^3 deduced from multiple echo experiments, using the demagnetizing coefficient $\beta = 4\pi$. The calculated values of χ are shown for comparison.

with the experimental susceptibility deduced from $b = \gamma\beta M_0 T_2$ using the limiting value $\beta = 4\pi$. The use of $\beta = 4\pi$ is justified in this case because the size of the sample grains was always much greater than the pitch of the helix magnetization and hence could be considered as infinite when calculating the demagnetizing field. We note also the satisfactory Curie law behavior of the experimental susceptibility reported in Fig. 7.

The same kind of comparison between the experimental data and the corresponding theoretical calculations is presented in Figs. 8–10 for a sample of solid ^{3}He maintained at fixed temperature $T = 402$ mK and placed in three different field gradients. These results demonstrate the crucial enhancement of the diffusion effect when the gradient increases. The deduced values of the diffusion coefficient D, as reported in Table II, are in agreement with earlier published data.[25] We note again that the measured susceptibility deduced from the fit using $\beta = 4\pi$ is equal to that calculated to less than 1%. The surprisingly small difference between the relaxation times of the two different molar volume samples considered here, $V_m = 23$ cm^3 and $V_m = 23.6$ cm^3, may be accounted for by the anisotropy effect expected in these single crystals; however more precise and independent measurements of T_2 are necessary to be more confident of this point.

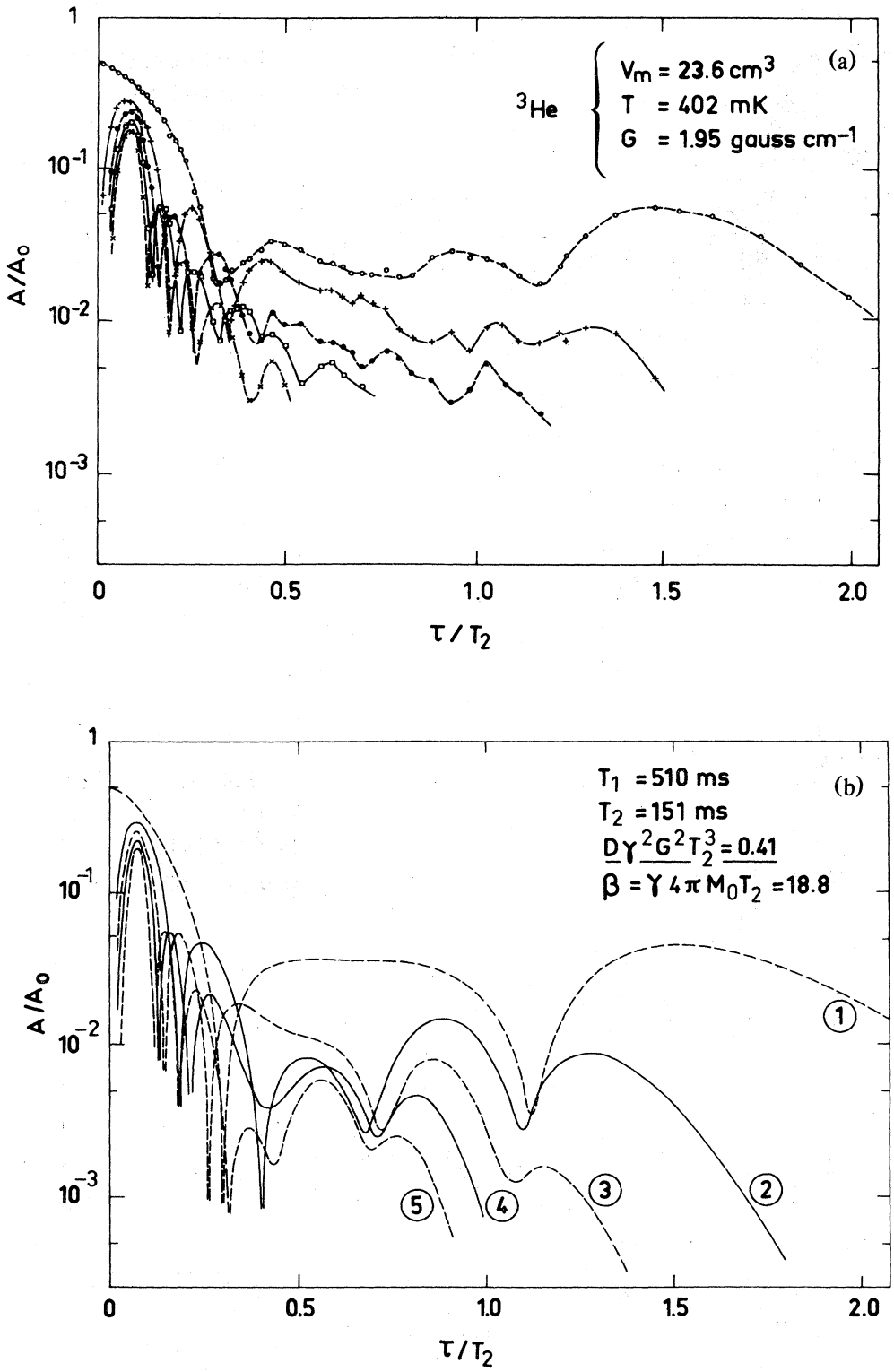

FIG. 8. Experimental (a) and calculated (b) amplitudes of the multiple echoes for a given sample ($V_m = 23.6$ cm^3) at $T = 402$ mK, $H_0 = 9250$ G ($\Omega_0/2\pi = 30$ MHz), when the applied field gradient is $G = 1.95$ G cm^{-1}.

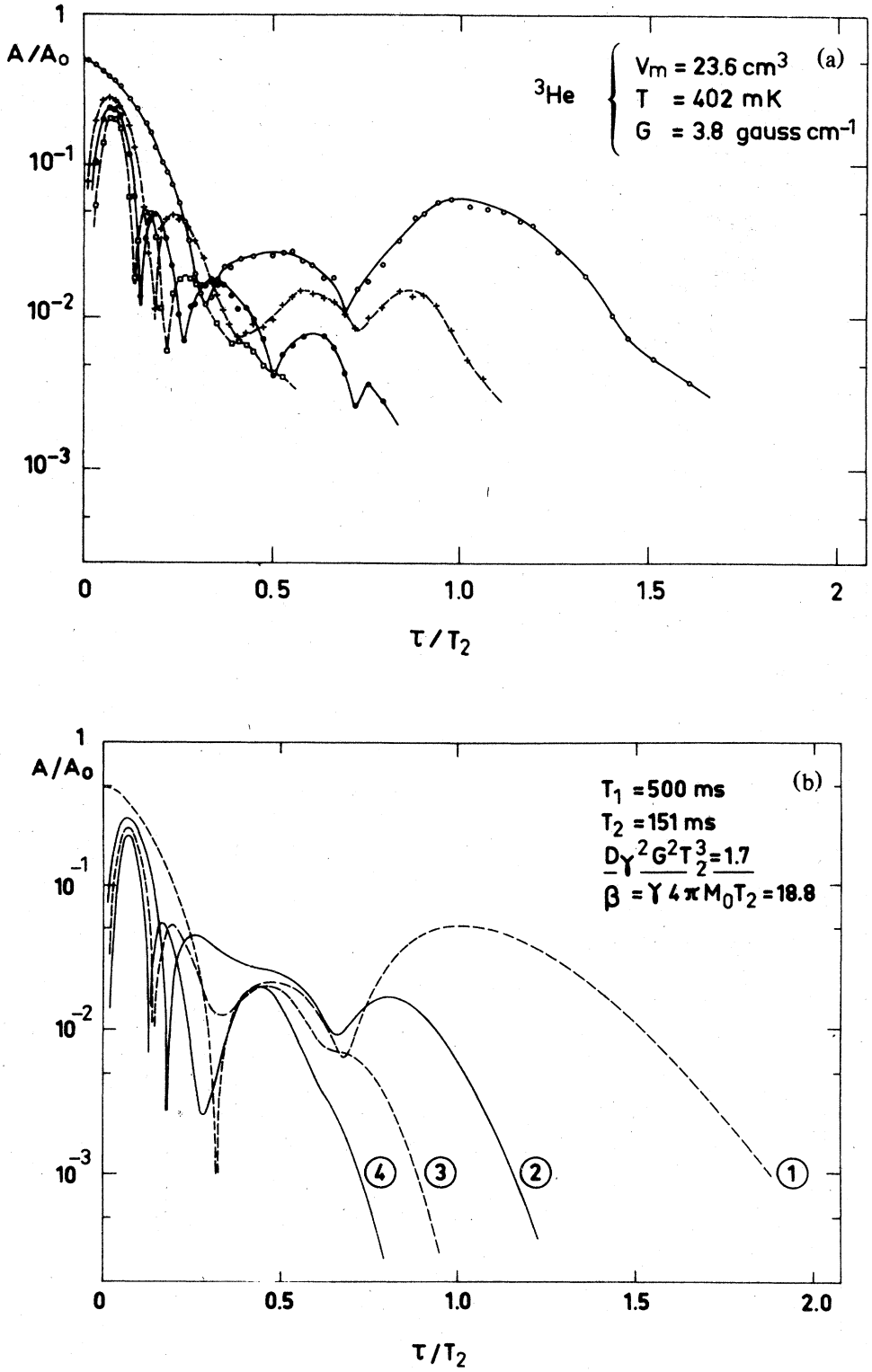

FIG. 9. Multiple echoes for the sample of Fig. 8 when the applied field gradient is $G = 3.8$ G cm^{-1}. (a) and (b) give the experimental and calculated amplitudes, respectively.

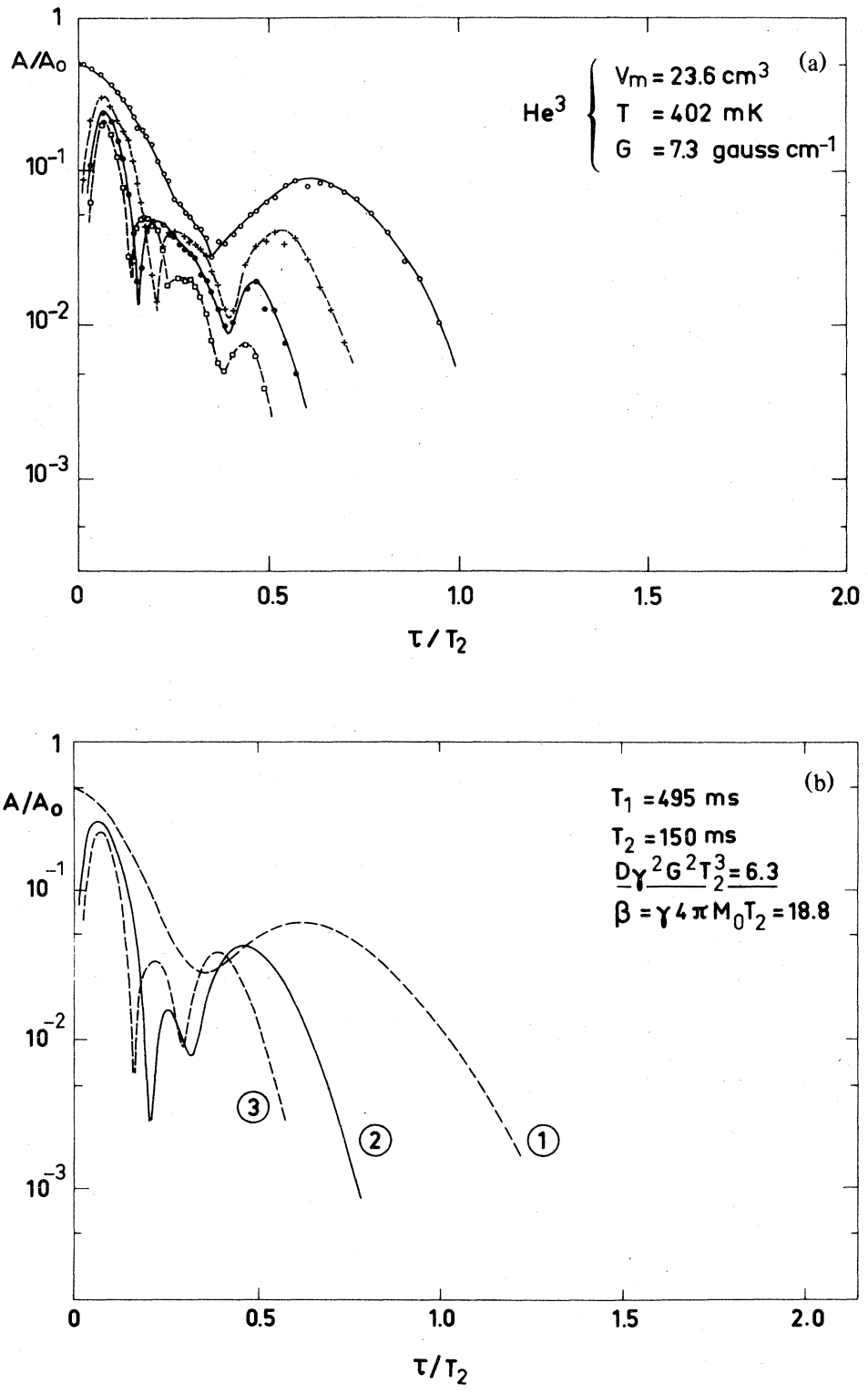

FIG. 10. Multiple echoes for the sample of Fig. 8 when the applied field gradient is $G = 7.3$ G cm^{-1}. (a) and (b) give the experimental and calculated amplitudes, respectively.

TABLE II. Longitudinal and transverse relaxation times T_1 and T_2, magnetic susceptibility χ, and diffusion coefficient D as determined by the analysis of the multiple-echo data reported in Figs. 8–10, for a given sample placed in three different field gradients. The determination of the calculated and measured magnetic susceptibilities was made as explained in Table I. As expected, the three experiments measure the same magnetization M_0.

^{3}He, $V_m = 23.6$ cm^3						
T (mK)	G (G cm^{-1})	T_1 (msec)	T_2 (msec)	$b = \gamma 4\pi M_0 T_2$	$\frac{\chi_{measured}}{\chi_{calculated}}$	D (10^{-8} cm^2 sec^{-1})
402	1.95	510	151	18.8	0.99	7.6
402	3.8	500	151	18.8	0.99	8.2
402	7.3	495	151	18.8	0.99	8.3

C. Analysis of the low-temperature data

We made the same kind of analysis as presented above, determining T_2, D, and M_0 by adjusting these parameters in the theoretical calculation of the echo amplitudes. Figures 11(a) and 11(b) are an example of the comparison between the data and the calculated curves. T_2 was found to be constant and equal to $T_1 = 250$ ms for all temperatures between 20.5 and 1.07 mK. As for the high-temperature experiments, we determined the magnetic susceptibility χ using $\beta = 4\pi$. The values of T_2, D, and χ are reported in Table III. The enhancement of the susceptibility when the temperature approaches the ordering temperature agrees with other published data[30,31] and we show in Fig. 12 the comparison between our χ values and the Prewitt-Goodkind values[31] obtained by SQUID measurements. The diffusion coefficient D was found to be constant within less than 10% in the whole temperature range considered. This surprising result has already been reported elsewhere[11] and compared with the predictions of the various theories for solid ^{3}He. In this paper devoted to the explanation of the multiple echoes, we only want to point

TABLE III. Longitudinal and transverse relaxation times T_1 and T_2, magnetic susceptibility χ, and diffusion coefficient D as determined by the analysis of the multiple-echo data obtained at low temperature with a sample formed in a Pomeranchuk cell. The absolute value of D is not accurate, owing to the lack of precise knowledge of the experimental field gradient; nevertheless D is constant to better than 10% in the temperature interval 20.5–1.07 mK. The magnetization M_0 varies by a factor 10 in the same interval. The experimental magnetic susceptibility was obtained using a demagnetizing coefficient β equal to 4π while the calculated magnetic susceptibility was obtained using $\chi_{calc} = NI(I+1)\gamma^2\hbar^2/3k_B T$, where N is the number of spins per unit volume. The ratio $\chi_{measured}/\chi_{calculated}$ emphasizes the increase of susceptibility in the paramagnetic phase when approaching the spin ordering temperature.

^{3}He, $V_m \sim 24.25$ cm^3 (melting curve)				
T (mK)	$T_1 = T_2$ (msec)	$b = \gamma 4\pi M_0 T_2$	$\frac{\chi_{measured}}{\chi_{calculated}}$ with $\Theta = -2.6$ mK	D (10^{-8} cm^2 sec^{-1})
20.5	250	2.25 ± 0.25	1.01	~ 15
10.5	250	4.05 ± 0.3	1.04	~ 15
4.45	250	9.0 ± 0.5	1.24	~ 15
2.54	250	13.3 ± 0.8	1.33	~ 15
1.47	250	20 ± 1	1.59	~ 15
1.07	250	23 ± 1	1.65	~ 15

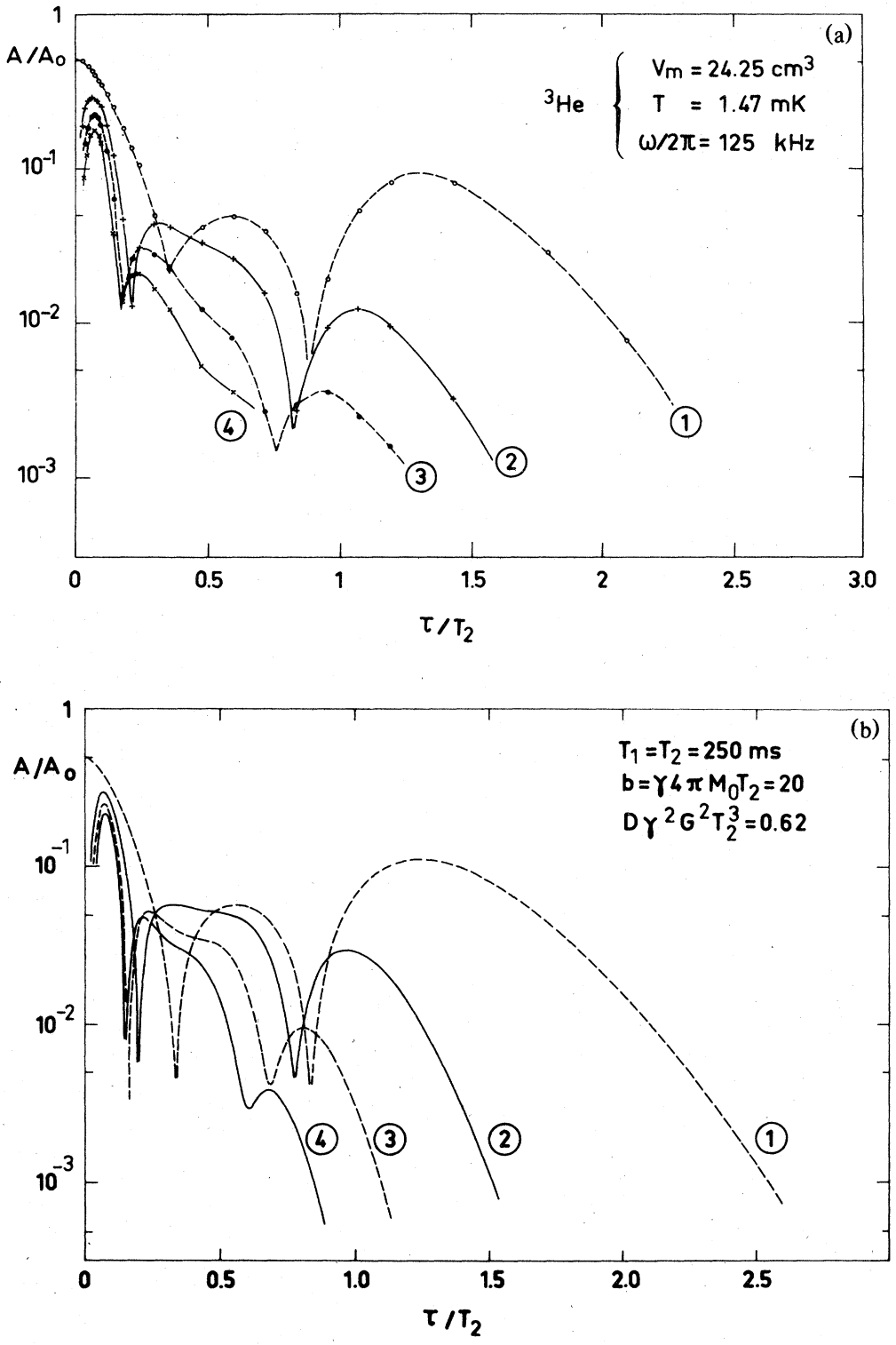

FIG. 11. (a): Experimental amplitudes of the multiple echoes for a sample cooled in a Pomeranchuk cell ($V_m \sim 24.25$ cm^3) at $T = 1.47$ mK and at low field ($H_0 = 38.6G$, $\Omega_0/2\pi = 125$ kHz). (b) gives the corresponding calculated amplitudes using the theory exposed in Sec. II D.

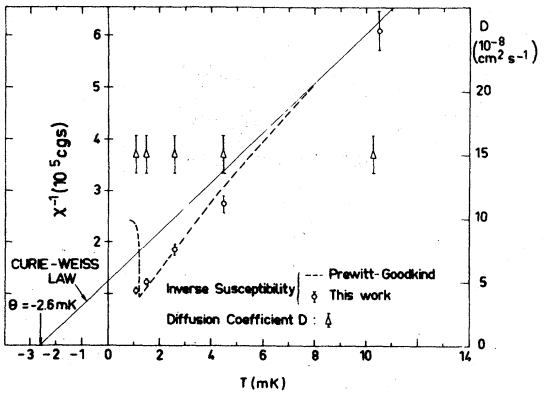

FIG. 12. Solid ^{3}He on the melting curve ($V_m = 24.25$ cm^3) in the vicinity of the spin ordering transition: the inverse susceptibility χ^{-1} and the diffusion coefficient D are determined by the multiple echo analysis as explained in the text. The figure is taken from Ref. 11; it compares our (χ^{-1}) result with the Curie-Weiss behavior and with the results of Prewitt and Goodkind (Ref. 31) obtained by SQUID measurement. The spin diffusion coefficient D is found to be constant even near the spin ordering transition.

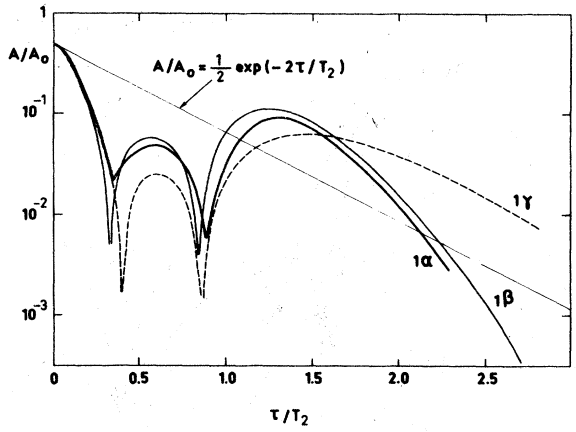

FIG. 13. Comparison of the analysis of the data when taking into account the diffusion and when neglecting it. The curve (1α) reproduces the experimental amplitude of the first echo of Fig. 11(a). The curve (1β) gives the corresponding calculated amplitude as it appears in Fig. 11(b) of this paper. The curve (1γ) gives the calculated amplitude of the first echo when the diffusion effect is neglected, as it appeared in Fig. 2 of the Ref. 2. The experimental conditions are: $V_m \simeq 24.25$ cm^3, $T = 1.47$ mK, $H_0 = 38.6$ G, $G = 0.8$ G cm^{-1}. The straight line gives the expected amplitude of the first echo in the absence if demagnetizing field (usual spin echo). As in Fig. 6(b), we note the amplification due to the demagnetizing field in the time interval: $T_2 < \tau < 2.3T_2$.

out that taking the diffusion into account improves significantly the agreement between theory and experiment; this point is illustrated in Fig. 13 where we compare the experimental amplitudes of the first echo (1α) at $T = 1.47$ mK and the corresponding calculated amplitudes with and without diffusion (1β and 1γ, respectively). When diffusion is taken into account it is easier to obtain an agreement between theory and experiment and hence, the susceptibility is also determined more precisely. The straight line gives the amplitude of the first echo in the absence of demagnetizing field and diffusion ($D = b = 0$); it emphasizes the amplification due to the action of the demagnetizing field, which appears clearly in this case for $1 < \tau/T_2 < 2.3$.

We point out that the multiple echo method determines the absolute value of the susceptibility as it is sensitive to the magnetization M which is an intensive quantity when usual methods measure the magnetic moment of a sample, which is an extensive quantity. Thus, in Fig. 12, we were not obliged to normalize our low-temperature data with the extrapolated high-temperature one as it is usually done when the experiments yield only relative values of M. Consequently, our χ results are plotted on an absolute scale while the Prewitt-Goodkind data are scaled according to the absolute Curie-Weiss law with $\Theta = -2.6$ mK.

The results presented in this section show that the multiple echo method can clearly provide interesting physical results for ^{3}He at very low temperature.

D. Discussion of the results

1. Results when the condition (4) prescribing a strong linear field gradient is not fulfilled

The comparison between theoretical and experimental multiple echo behavior shows evidently that the agreement is not always perfect. For instance the initial decrease of the first echo (at short τ) is always faster in the theoretical curve than in the experimental curve [see for example Figs. 6(a) and 6(b)]. At larger τ, the experimental decrease of high-order echoes disagrees with the theory [see Figs. 8(a) and 8(b), for example]. We believe that these discrepancies are mainly due to the fact that the field gradient was not perfectly uniform over the sample and that consequently the behavior of the magnetization was not described by a real one-dimensional equation.

We already mentioned in Sec. II that an apparently very fast longitudinal relaxation of M_z may appear after the second pulse, which could be misinterpreted as a fast intrinsic T_1 relaxation. An example of such a behavior is shown in Fig. 14. We see that the free induction decay following the second rf pulse rises ra-

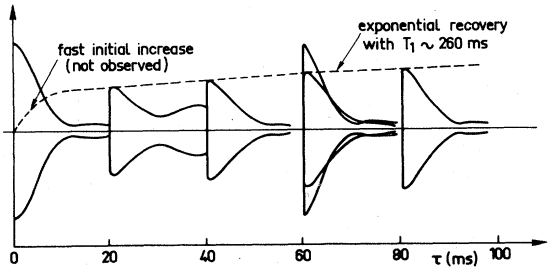

FIG. 14. Example of the anomalous behavior of the free precession signal following the second 90° rf pulse when the applied field gradient is smaller than the minimal value required by the condition (4) of Sec. II. This figure represents a multiple exposure picture where the second pulse is applied at times $\tau = 20$, 40, 60, and 80 msec. The deformation of the second free precession signal is emphasized at $\tau = 60$ msec by superimposing on it the first free precession signal. This shows clearly that the two signals are not proportional. The dotted line gives the envelope of the second free precession when τ varies; for $\tau > 15$ msec, the exponential increase defines the usual longitudinal relaxation time T_1 but at short times, the increase is much faster, though hidden by the first free precession signal. These signals were obtained at $T = 1.5$ mK and $\omega/2\pi = 125$ kHz for a solid ^{3}He in contact with liquid in the Pomeranchuk cell.

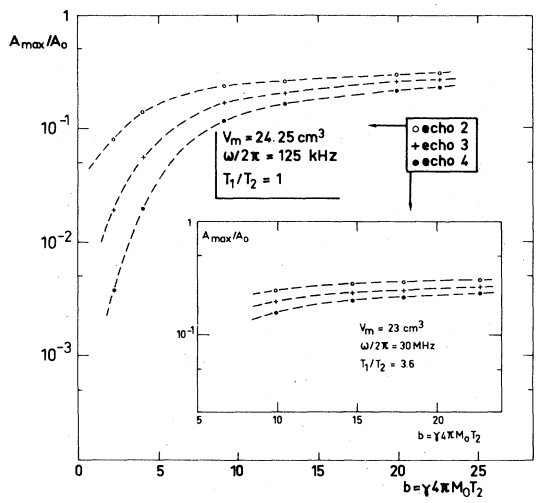

FIG. 15. Calculated first maximum amplitudes of the echoes 2, 3, and 4, as a function of the parameter $b = \gamma 4\pi M_0 T_2$. When $b \leq 10$, they are very sensitive to the value of b and hence, they can be used to determine this parameter. The reported values are taken from the theoretical curves $3b$ to $6b$ for the inset and from similar calculated curves corresponding to the low-temperature data for the others.

pidly at short τ and that its shape is different from that of the first free induction decay. In short the explanation is the following: when the field gradient is so small that the condition (4), $4\pi M_0 << Gl$ is not satisfied, the transverse precession becomes very complicated and depends on the shape of the sample. As the magnetization is no more unidimensional, the transverse component of the magnetization and the demagnetizing field are no longer parallel in all parts of the sample. Thus, the local precession of the transverse magnetization around the transverse demagnetizing field produces a longitudinal magnetization which appears during the characteristic time of the free precession. This initial rapid increase of M_z is illustrated by the dashed line in Fig. 14. For a quantitative analysis of multiple-echo behavior, this complex effect must be suppressed and this can be done by increasing the magnetic field gradient G.

2. *Clue for a rapid evaluation of the magnetization*

The determination of M_0 and D discussed in Sec. III D 1 has been obtained using the entire multiple-echo pattern. We would now like to show how to determine the magnetization M_0 if one knows only the short-time behavior of the multiple echoes. This point is illustrated in Figs. 15 and 16. Figure 15 shows the normalized first maximum amplitudes A_{max}/A_0 for the echoes 2, 3, and 4, as a function of the parameter $b = \gamma 4\pi M_0 T_2$. When $b \gtrsim 10$, these amplitudes are nearly constant as b varies (the same is true when $T_1/T_2 \neq 1$, as shown in the inset). When $b \lesssim 5$, as the whole echo pattern varies smoothly with b, the precise determination of M_0 may become difficult to obtain, but Fig. 15 shows

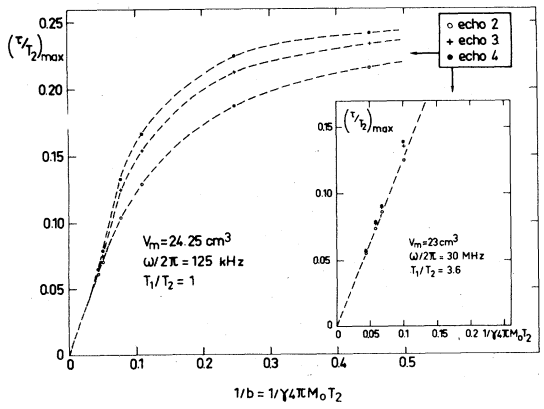

FIG. 16. Positions of the maximum amplitudes of the echoes 2, 3, and 4, as a function of the parameter $b = \gamma 4\pi M_0 T_2$. When $b \gtrsim 10$, they can be used to determine the parameter b. This property is still valid when T_1/T_2 is different from 1, as shown in the inset.

that, in this case, the maximum amplitudes of the successive echoes which are strongly sensitive to b, can be used to determine this parameter. On the other hand, Fig. 16 shows that the position $(\tau/T_2)_{max}$ of the successive maxima of the echoes can be used to determine the parameter b for high values of b. Thus, according to whether b is low ($\lesssim 5$) or high ($\gtrsim 10$) it can be determined rather accurately by considering either the amplitudes or the positions of the first maxima of the echoes 2, 3, 4,....

IV. CONCLUSION

In this paper a complete solution of the equation of motion of the magnetization of solid ^{3}He in the paramagnetic phase has been presented, including the non-negligible effect of the nonlinear term due to the demagnetizing field and the effect of the spin diffusion. It has been shown that this theory gives a satisfactory description of the experimental multiple echoes observed at high and low temperature. This calculation was carried out without physical simplification, except for the assumption—which was actually satisfied in the experiments—that the magnetization was a one-dimensional function of space variable, i.e., that the uniform magnetic field gradient was sufficiently large. Thus, this theory may be a useful quantitative example when considering the general problem of more complex nonlinear systems which were mentioned in the Introduction. We point out again that the main practical application of the multiple-echo phenomenon is the direct and absolute determination of the magnetization of a sample, without knowing the number of spins contained in it. The multiple-echo feature has provided the first measurement of the magnetization of solid ^{3}He near the ordering temperature[2] in a Pomeranchuk cell where the number of spins in the sample is strictly unknown. The susceptibility was found to be larger than the extrapolated Curie Weiss value, in contradiction with an antiferromagnetic Heisenberg model[12]; this behavior has been confirmed later by SQUID[31] and thermodynamic measurements.[30] We remark that the fundamental condition (5b)) $\gamma 4\pi M_0 T_2 > 1$ is fulfilled in very pure water at $H = 10$ kG and $T = 300$ K if $T_2 > 6$ sec; nevertheless the observation of the multiple echoes in water needs a very homogeneous magnetic field (the maximum field gradient allowed is of the order of 0.1 mG cm^{-1}, in order to avoid strong diffusion effects), which may be difficult to achieve for such an experiment which could be amusing but of little interest.

We mentioned in the Introduction that nearly the same spin precession equations also appear in uniaxial antiferromagnets[9] although the demagnetizing field is quite negligible. In these systems, the Shul-Nakamura interaction[32,33] induces a dynamic frequency shift of the resonance frequency proportional to the longitudinal spin magnetization, which is identical to the frequency shift in solid ^{3}He expressed by Eq. (10) of this paper. Thus, in principle, the same equations are valid in these substances and the same multiple echoes should be observed. Unfortunately there is a large experimental spread of values of b which smooths the zeroes of the Bessel functions and prevents the observation of a large number of echoes: in Ref. 9, the second echo is nearly undetectable and no well defined zero of Bessel function has been observed. Probably for the same reason, in all the physical systems where the same kind of multiple echoes is expected (plasmons, photons, phonons, etc . . .), it appears that the number of echoes actually observed is much smaller than the 40 echoes we can easily detect in solid ^{3}He.

In any pulse NMR experiments—in solid ^{3}He and probably in some other substances—one must always bear in mind the demagnetizing field effects even when using a single rf pulse, if the spin polarization is non-negligible. We point out that in the ferromagnetism of liquid ^{3}He in contact with a surface,[34,35] multiple echoes can occur, related to the demagnetizing field of the two large susceptibility layers near the surface. The observation of these multiple echoes could give some informations about this surface layer; spatial variation of χ and diffusion coefficient near the surface. However in a Pomeranchuk cell the signal due to the surface layers remains small compared to the solid signal. This prevented us to obtain any significant information about these layers.

ACKNOWLEDGMENTS

We thank G. Delmas for his help with the construction of the apparatus and F. I. B. Williams, N. Sullivan and M. Goldman for their suggestions and critical reading of the manuscript.

[1]E. Hahn, Phys. Rev. 80, 580 (1950).
[2]M. Bernier and J. M. Delrieu, in *Proceedings of the XIXth Congress Ampere on Magnetic Resonance and Related Phenomena,* edited by H. Brunner, K. H. Hausser, and D. Schweitzer (Groupement Ampère, Geneva, 1976).
[3]O. Avenel, P. Berglund, M. Bernier, J. M. Delrieu, E. Varoquaux, and C. Vibet, in *Proceedings of the XIXth Congress Ampere on Magnetic Resonance and Related Phenomana,* edited by H. Brunner, K. H. Hausser, and D. Schweitzer (Groupement Ampère, Geneva, 1976).
[4]M. Bernier and J. M. Delrieu, Phys. Lett. A 60, 156 (1977).
[5]N. S. Shiren, R. L. Melcher, D. K. Garrod, and T. G. Kazyaka, Phys. Rev. Lett. 31, 819 (1973).
[6]I. B. Goldberg, E. Ehrenfreund, and M. Weger, Phys. Rev. Lett. 20, 539 (1968); E. Ehrenfreund, I. B. Goldberg, and M. Weger, J. Appl. Phys. 39, 5941 (1968).
[7]G. F. Herrmann and R. F. Whitmer, Phys. Rev. 143, 122 (1966).
[8]J. Joffrin and A. Levelut, Phys. Rev. Lett. 29, 1325 (1972).
[9]Yu. M. Bun'kov and B. S. Dumesh, Zh. Eksp. Theor. Fiz. 68, 1161 (1975), [Sov. Phys. JETP 41, 576 (1975)].
[10]R. W. Gould, Phys. Lett. A 29, 347 (1969).
[11]G. Deville, J. M. Delrieu, and M. Bernier, J. Phys. Lett. (Paris) 39, 453 (1978).
[12]A. Landesman, J. Phys. (Paris) 39, C6-1305 (1978).
[13]J. H. Hetherington and F. D. C. Willard, Phys. Rev. Lett. A 20, 449 (1977).
[14]M. Roger, J. M. Delrieu, and A. Landesman, Phys. Lett. A 62, 449 (1977).
[15]M. Roger and J. M. Delrieu, Phys. Lett. A 63, 309 (1977).
[16]A. F. Andreev and I. M. Lifshitz, Zh. Eksp. Theor. Fiz. 56, 2057 (1969), [Sov. Phys. JETP 29, 1107 (1969)]; A. F. Andreev, V. I. Marchenko, and A. E. Meierovich, JETP Lett. 26, 36 (1977).
[17]M. Heritier and P. Lederer, J. Phys. Lett. (Paris) 38, 209 (1977).
[18]A. Abragam, *Principles of Nuclear Magnetism* (Oxford University, London, 1961), Chap. X.
[19]See for instance, A. Landesman, Ann. Phys. (Paris) 8, 53 (1974).
[20]See for instance, M. H. Cohen and F. Keffer, Phys. Rev. 99, 1128 (1955); A. J. Leggett, Rev. Mod. Phys. 47, 331 (1975).
[21]See Ref. 18, Chap. 3.
[22]A. Ralston and H. S. Wilf, *Mathematical Methods for Digital Computers* (Wiley, New York, 1960), Vol. I, p. 115; B. Carnahan, H. A. Luther, and J. O. Wilkes, *Applied Numerical Methods* (Wiley, New York, 1969), p. 363.
[23]A. B. Harris, Solid State Commun. 9, 2255 (1971).
[24]G. Deville, J. Phys. (Paris) 37, 781 (1976).
[25]R. L. Garwin and H. A. Reich, Phys. Rev. 115, 1478 (1959); H. A. Reich, Phys. Rev. 129, 630 (1963).
[26]J. E. Vos, B. S. Blaisse, D. A. E. Bóon, W. J. Van Scherpenzeel, and R. Kingma, Physica (Utrecht) 37, 51 (1967); J. E. Vos and R. Kingma, Cryogenics 7, 50 (1967); J. E. Vos, R. Veenenga Kingma, F. J. Van der Gaag, and B. S. Blaisse, Phys. Lett. A 24, 738 (1967).
[27]L. P. Mezhov Deglin, Zh. Eksp. Theor. Fiz. 49, 66 (1965), [Sov. Phys. JETP 22, 47 (1966)].
[28]R. H. Crepeau, O. Heybey, D. M. Lee, and S. A. Strauss, Phys. Rev. A 3, 1162 (1971).
[29]D. Marty and F. I. B. Williams, J. Phys. (Paris) 34, 989 (1973).
[30]D. M. Bakalyar, C. V. Britton, E. D. Adams, and Y. C. Hwang, Phys. Lett. A 64, 208 (1977).
[31]T. C. Prewitt and J. M. Goodkind, Phys. Rev. Lett. 39, 1283 (1977).
[32]H. Shul, Phys. Rev. 109, 606 (1958).
[33]T. Nakamura, Progr. Theor. Phys. 20, 542 (1958).
[34]A. I. Ahonen, T. Kodama, M. Krusius, M. A. Paalanen, R. C. Richardson, W. Schoepe, and Y. Takano, J. Phys. C 9, 1665 (1976).
[35]M. T. Beal-Monod and S. Doniach, J. Low Temp. Phys. 28, 175 (1977).

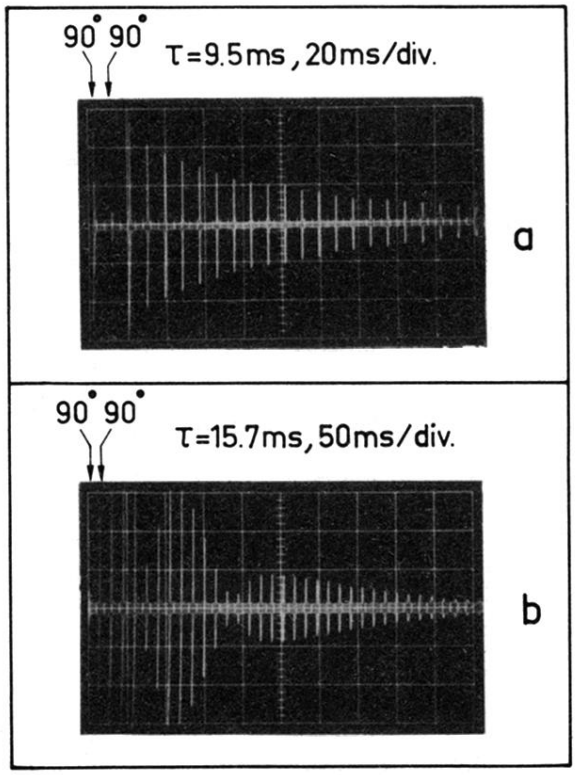

FIG. 2. Photographs of typical multiple echo patterns obtained for two values of the time interval τ between the 90° radio-frequency pulses. The temperature was $T = 320$ mK, the magnetic field was $H_0 = 9250$ G and the molar volume was $V_m = 23.6$ cm^3. At $\tau = 9.5$ msec, there is no minimum amplitude for any echo. At $\tau = 15.7$ msec, the echoes 4 and 12 reach their first and second minimal amplitude, respectively, so that the behavior of the whole pattern is strongly nonmonotonic. Owing to the strong field gradient, the free precession following the two pulses are narrow, thus the recovery time of the receiver prevents the observation of their early decay. Consequently, the observed free precession appearing in these photographs are not scaled with the echoes. Compared with Fig. 2(a), the gain is multiplied by 7 in Fig. 2(b).